Development and Validation of a Finite Element Model of the THOR Lower Extremity

Final Report

April, 2004

John Varellis, Ph.D.
J. Quinn Campbell
Rabih E. Tannous, Ph.D.

AASA Inc.
www.aasainc.com

TABLE OF CONTENTS

LIST OF FIGURES

LIST OF TABLES

ABSTRACT

A three-dimensional finite element model was developed to represent the response of the THOR lower extremity (THOR-LX). CAD drawings of the THOR-LX hardware were used to construct the geometry of the model. Most of the components were modeled as rigid bodies, with the exceptions of the tibia skin, foot skin, tibia compliance spring, the heel padding/shoe, and the Achilles' cable. To account for the movement of the lower extremity, one translational joint was created for compression of the tibia and three revolute joints were created to allow movement of the ankle. Stiffness and damping properties were assigned for each of the joints to represent the mechanical properties in the physical THOR-LX. The finite element model outputs the same measurements as the THOR-LX dummy: load cells, two accelerometers, and rotation angles of the ankle. The completed finite element model was correlated with the physical THOR-LX by simulating ten physical experiments and comparing the results. Three impacts to the ball of the foot were conducted to evaluate the dorsi joint performance. Two heel impacts were performed to evaluate the tibia compliance. Three Achilles' tests were conducted to assess the Achilles' cable forces. Two skin tests were performed to determine the effect of the skin on the tibia forces. The time histories for impactor deceleration, load cell forces, and joint angles and moments calculated for these tests all compared well to the experimental data. Therefore, it is concluded that the finite element model can be used to accurately predict the results of physical tests performed with the THOR-LX.

INTRODUCTION

The THOR (Test device for Human Occupant Restraint) dummy was developed as the next generation in crash test dummies. The THOR-LX is the lower extremity used with the THOR dummy. THOR-LX is an improvement over previous anthropometric lower extremities, especially the Hybrid III leg, because it is more biofidelic and has additional instrumentation. Some of these advances include: 1.) axial compliance to represent compressibility of the tibia, 2.) a fully functioning ankle that allows rotation in all three directions and 3.) an Achilles' cable that provides an alternate load path in the lower leg and controls dorsiflexion. Furthermore, there are two load cells and two accelerometers. The upper load cell monitors Fx, Fz, Mx, and My while the lower monitors Fx, Fy, Fz, Mx, and My. The tibia accelerometer measures Ax and Ay while the foot accelerometer measures Ax, Ay, and Az. These improvements make the THOR-LX the most advanced experimental tool available for predicting injuries to the lower extremity. However, with the increasing use of computer modeling, a validated finite element model of the THOR-LX can also be an important tool to predict injury to the physical lower extremity. The purpose of this report is to present the design and validation of the THOR-LX finite element model.

MODEL DESCRIPTION

The THOR-LX finite element (FE) model was developed for use in LS-DYNA 3D. The model is based on a basic lower leg model developed by the Volpe National Transportation Systems Center (Zhou et al. 2002). While the underlying structure of the model is similar to the Volpe model, many modifications and improvements have been made. The geometry is based on CAD drawings of the actual THOR-LX hardware. The THOR-LX FE model (Figure 1) consists of 3521 hexagonal elements, 96 seatbelt elements, 1 discrete spring element, and 7614 nodes. 45% of the elements are deformable and the remaining 55% are rigid. A variety of techniques are used to model the interface between the different parts of the model including: joints, rigid body merge sets, contact definitions, and extra nodes to rigid bodies. While most of the parts in the

physical THOR-LX are represented explicitly, some parts are simplified to increase the model's solution speed and stability while maintaining accurate behavior of the model.

Figure 1. The THOR-LX FE model.

Model Structure

The THOR-LX FE model consists of the following basic sub-assemblies (Figure 2): knee clevis and upper tibia area, lower tibia area, lower tibia load-cell and top torque base, ankle joint, foot assembly, and Achilles' assembly. Since most of the parts of the THOR-LX are considered rigid, several of these parts have been grouped into rigid body merge sets and linked with joints. The upper tibia area and lower tibia area are connected with a translational joint. The lower tibia area and the lower tibia load cell are attached with a locking joint. The top and bottom of the ankle joint are rigidly merged with the top torque base and foot assembly respectively. The ankle joint itself consists of three revolute joints, thus allowing it to rotate in all three anatomical directions.

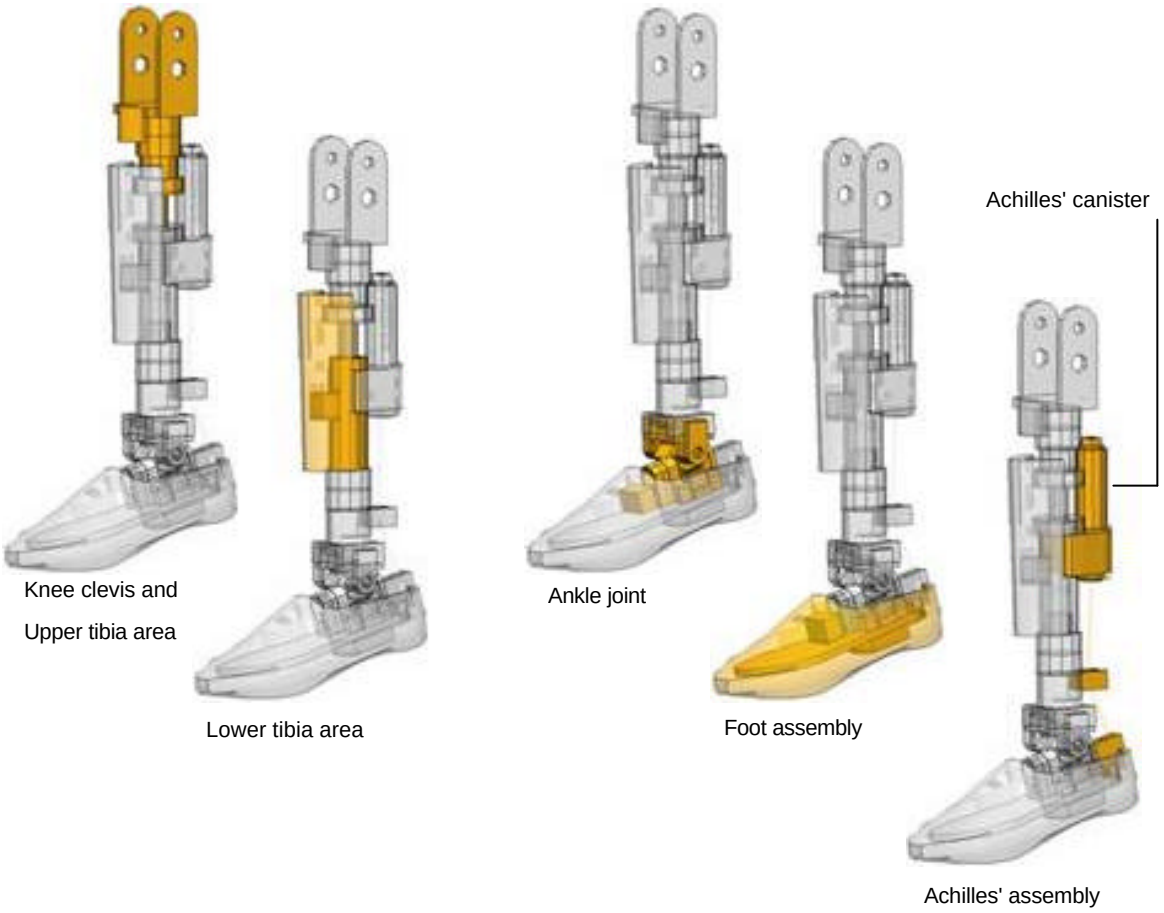

Figure 2. Structural Sub-Assemblies.

The deformable parts in the model are primarily connected using extra nodes. Extra nodes connected to the rigid body are used to hold the Heel Pad onto the Composite Foot sole, the Tibia Skin onto the tibia, and the Foot Skin onto the Composite Foot Sole.

There are also two types of contacts defined to model the interface of parts in the FE model for THOR-LX (Figures 3 and 4). These are:

1. *CONTACT_AUTOMATIC_SURFACE_TO_SURFACE is defined between the inner surface of the contoured foot and the heel padding

2.*CONTACT_AUTOMATIC_SINGLE_SURFACE is defined between the leg skin, the tibia guard and the knee bumper.

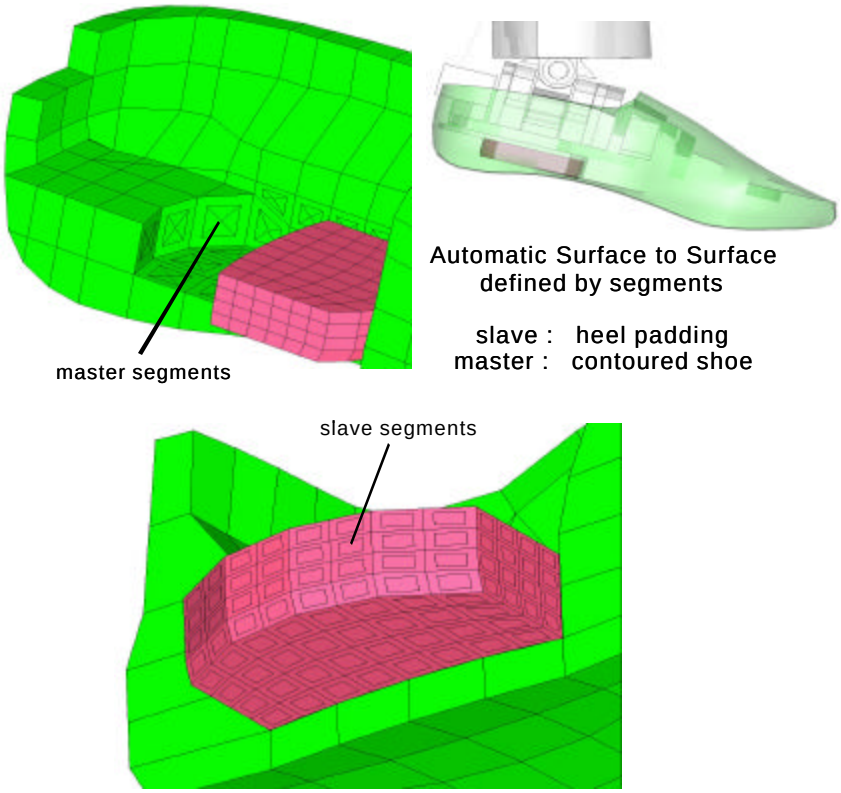

Figure 3. Picture showing contact interfaces on the heel pad.

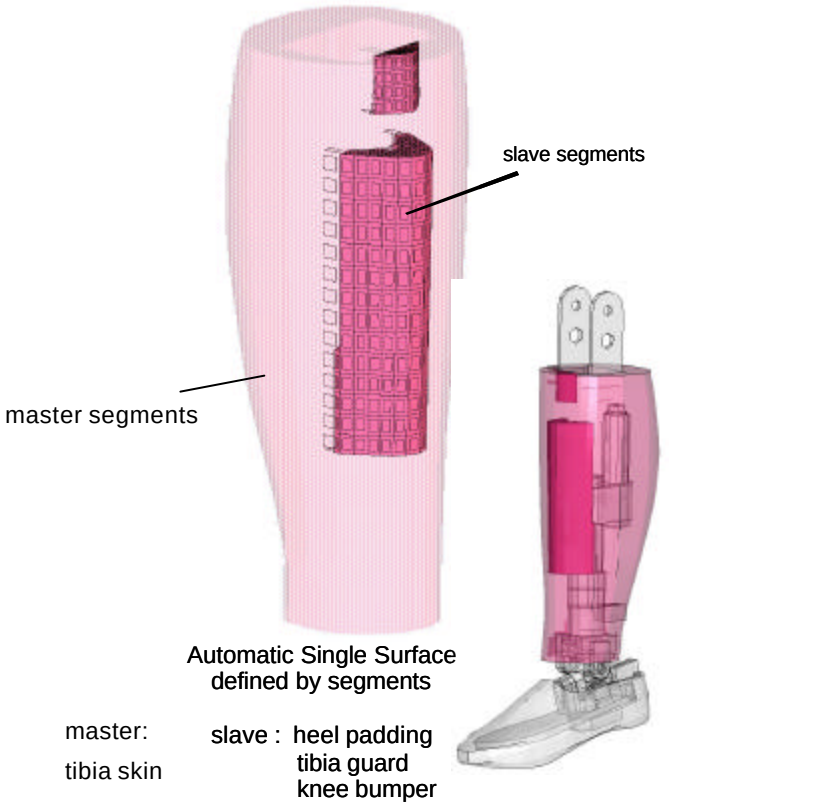

Figure 4. Defined sliding interfaces in the THOR-LX tibia guard.

Material Characteristics

The only deformable parts found in the THOR-LX FE model are the tibia skin, foot skin, tibia compliance spring, the heel padding/shoe, and the Achilles‘ cable. The skin for both the foot and leg is modeled as an elastic material. The tibia compliance spring and the heel padding are each represented by viscoelastic materials. The Achilles’ cable uses a deformable seatbelt material that will be discussed in more detail in the section on modeling techniques. Most of the other parts in the physical THOR-LX are made out of Aluminum and are modeled with a rigid material in the FE model. Table 1 lists each component in the FE model, along with its material formulation, element formulation, mass, and material properties.

Modeling Techniques

As previously stated, a variety of modeling techniques were used to represent the THOR-LX components in the finite element model. These techniques were selected to allow for faster and more stable solutions. One such technique is seen where the neoprene tibia bushing found in the dummy, which allows for compression of the tibia, is not explicitly modeled. It has been replaced in the FE model by a translational joint that allows the lower and upper tibia areas to slide along the tibia axis. Resistance is instead provided by a viscoelastic tibia compliance spring, shown in Figure 5.

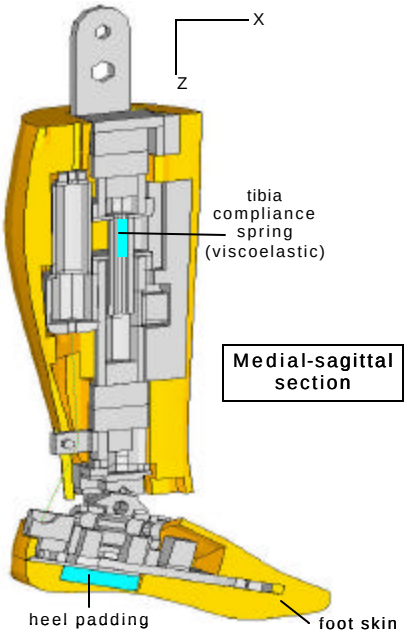

Figure 5: Location of the Tibia Compliance Spring in the model.

Table 1. THOR-LX Material properties. (Mass (kg), E = Young's Modulus (Mpa), K = bulk modulus (Mpa), G_8 = long term shear modulus (Mpa), G_0 = short term shear modulus (Mpa), B = viscoelastic time constant (1/sec), K_0 = short term bulk modulus (Mpa), K_8 = long term bulk modulus (Mpa).

Component Name	Material Type	Physical Property	Mass	E	K	G_8	G_0	B	K_0	K_8
Knee_Clevis	Rigid	Solid	0.23700	69000	-	-	-	-	-	-
Molded_Knee_Bumper	Rigid	Solid	0.01110	5000	-	-	-	-	-	-
upr_Tibia_LoadCell1	Rigid	Solid	0.23900	207000	-	-	-	-	-	-
upr_Tibia_LoadCell2	Rigid	Solid	0.31100	207000	-	-	-	-	-	-
upr_Tibia_Tube	Rigid	Solid	0.05820	72000	-	-	-	-	-	-
Tibia_Comp _Bush_Plunger	Rigid	Solid	0.22800	207000	-	-	-	-	-	-
Tibia_Bushing_Spring	Viscoelastic	Discrete	0.00000	-	-	-	-	1000	1000	200
Tibia_Comp_Bush_lwr_Flange	Rigid	Solid	0.04230	69000	-	-	-	-	-	-
lwr_Tibia_Tube	Rigid	Solid	0.18000	72000	-	-	-	-	-	-
Tibia_TriAxial_Mountng_Plate	Rigid	Solid	0.00739	69000	-	-	-	-	-	-
Tibia_TriAxial_Accelerometer	Rigid	Solid	0.06500	207000	-	-	-	-	-	-
Tibia_Guard	Rigid	Solid	0.24300	5000	-	-	-	-	-	-
lwr_Tibia_LoadCell1	Rigid	Solid	0.31200	207000	-	-	-	-	-	-
lwr_Tibia_LoadCell2	Rigid	Solid	0.27900	207000	-	-	-	-	-	-
top_Torque_Base	Rigid	Solid	0.19100	69000	-	-	-	-	-	-
Dorsi_Plantar_SoftStop_Base	Rigid	Solid	0.01760	69000	-	-	-	-	-	-
Dorsi_Plantar_Soft_Stop	Rigid	Solid	0.00586	14.52	-	-	-	-	-	-
top_Torque_Base_Cap	Rigid	Solid	0.02810	69000	-	-	-	-	-	-
side_Ankle_Bushing_Plates	Rigid	Solid	0.02960	69000	-	-	-	-	-	-
side_Ankle_PotentiomtrCover	Rigid	Solid	0.00918	3100	-	-	-	-	-	-
PM_tibia_bushing	N/A	N/A	0.03600	-	-	-	-	-	-	-
Achilles_Pulley	Rigid	Solid	0.06580	207000	-	-	-	-	-	-
Achilles_Spring_Tube_Base	Rigid	Solid	0.17600	72000	-	-	-	-	-	-
Achilles_Spring_Tube	Rigid	Solid	0.06700	69000	-	-	-	-	-	-
Achilles_Retaining_Nut	Rigid	Solid	0.02740	207000	-	-	-	-	-	-
Torque_Base_CenterBlock	Rigid	Solid	0.05810	69000	-	-	-	-	-	-
Eversion_Inversion_SoftStop	Rigid	Solid	0.00577	14.52	-	-	-	-	-	-
Evers_Invers_SoftStop_Base	Rigid	Solid	0.01430	69000	-	-	-	-	-	-
btm_Torque_Base_Cap	Rigid	Solid	0.02810	69000	-	-	-	-	-	-
btm_Torque_Base	Rigid	Solid	0.07530	69000	-	-	-	-	-	-
fraft_Ankle_Bushing_Plates	Rigid	Solid	0.02960	69000	-	-	-	-	-	-
frnt_Ankle_PotentiomtrCover	Rigid	Solid	0.00918	3100	-	-	-	-	-	-
Foot_Composite_Sole	Rigid	Solid	0.17700	50000	-	-	-	-	-	-
Heel_Padding	Viscoelastic	Solid	0.03480	-	160	1	0.5	700	-	-
Foot_TriAxial_Mountng_Plate	Rigid	Solid	0.00520	69000	-	-	-	-	-	-
Foot_TriAccelerometer	Rigid	Solid	0.03890	72000	-	-	-	-	-	-
Foot	Elastic	Solid	0.32500	100	-	-	-	-	-	-
Achilles_Heel_Mountng_Post	Rigid	Solid	0.03140	69000	-	-	-	-	-	-
Achilles_lwr_Mountng_Post	Rigid	Solid	0.05460	69000	-	-	-	-	-	-
Achilles_Cable1	Seatbelt	Seatbelt	0.00299	-	-	-	-	-	-	-
Achilles_Cable2	Seatbelt	Seatbelt	0.00306	-	-	-	-	-	-	-

A second modeling technique is used for the ankle. The THOR-LX has a multifunctional ankle joint able to perform all three rotations of the human ankle (Figure 6): dorsi and plantar flexion, eversion and inversion, internal and external rotation. The ankle in the physical THOR-LX has three soft stops that provide resistance to ankle rotation. Before the Torque Base Center Block (Figure 7) hits the soft stop, the rotation is opposed by rubber supports at both ends of the physical pin. When the Torque Base Center Block hits the soft stop, the rotation does not stop. The soft stop is compressed, further opposing the rotation of the Torque Base Center Block, until the soft stop material bottoms out.

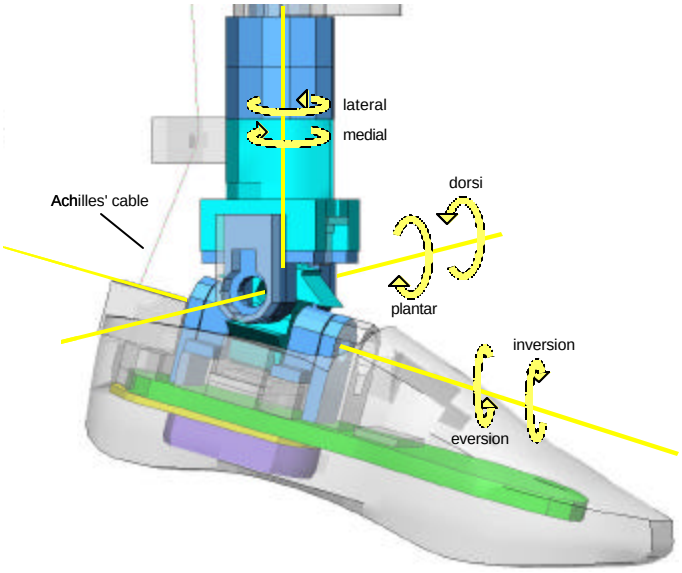

Figure 6. THOR-LX ankle, front left isometric view showing functionality.

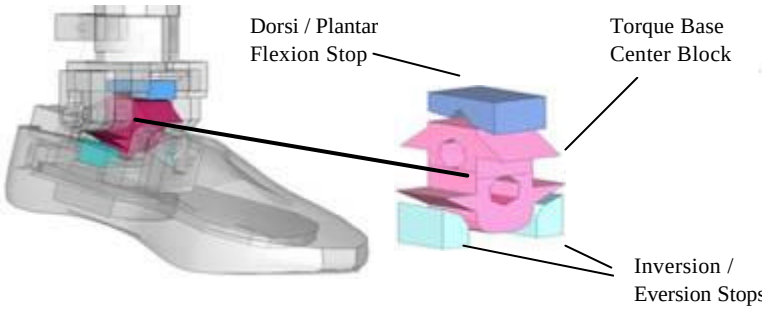

Figure 7. THOR-LX soft stops.

In the FE model, three revolute joints are used to represent the three rotations allowed at the ankle. The rubber supports at the two ends of the physical pin are not modeled. In addition, no contact is defined between the Torque Base Center Block and the soft stop. The rotational reaction on the pin and the soft stop action are both represented instead mathematically by adding the appropriate joint stiffness with damping. Figure 8 shows the moment curve as a function of angle for each joint in the ankle. The angle with a zero moment (or stress free state) for THOR-LX is when the foot assembly is in plantar flexion at 15 degrees below the Global X-Y plane (Figure 9).

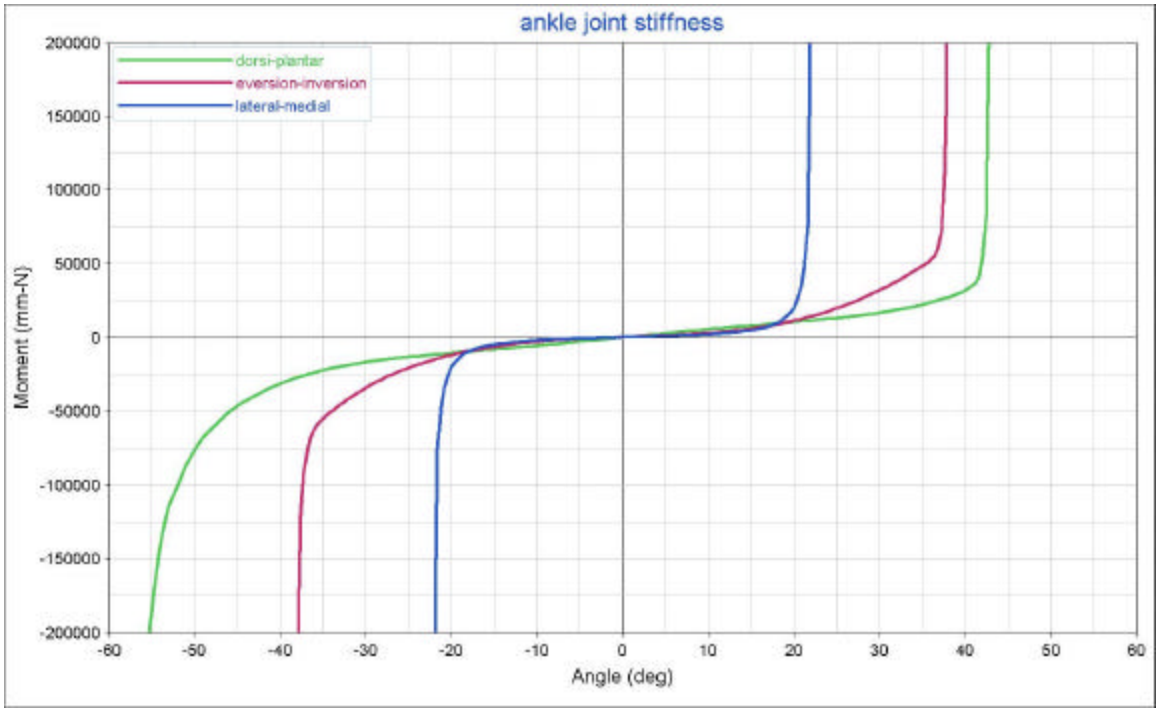

Figure 8. Mathematical joint stiffness curves for the THOR-LX ankle joints.

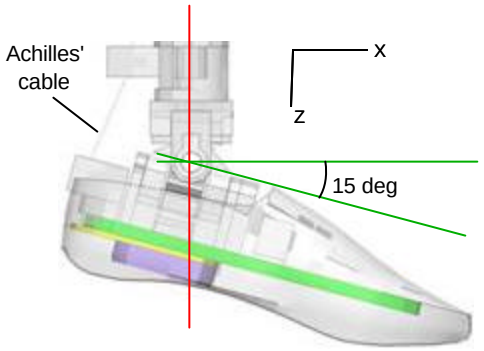

Figure 9. THOR-LX foot medial view neutral position.

Finally, the last modeling technique is used for the Achilles' cable and pulley. In the THOR-LX dummy, these components are used to provide an alternate load path in the lower leg and control dorsiflexion. The resistance in the physical Achilles' cable comes from the compression of soft foam, a coil spring, and a neoprene bushing inside the Achilles' canister. In the FE model, these parts are represented by seatbelt elements and a slip-ring, as shown in Figure 10. The Achilles' canister in the model is empty and the seatbelt represents the combined stiffness of the parts inside.

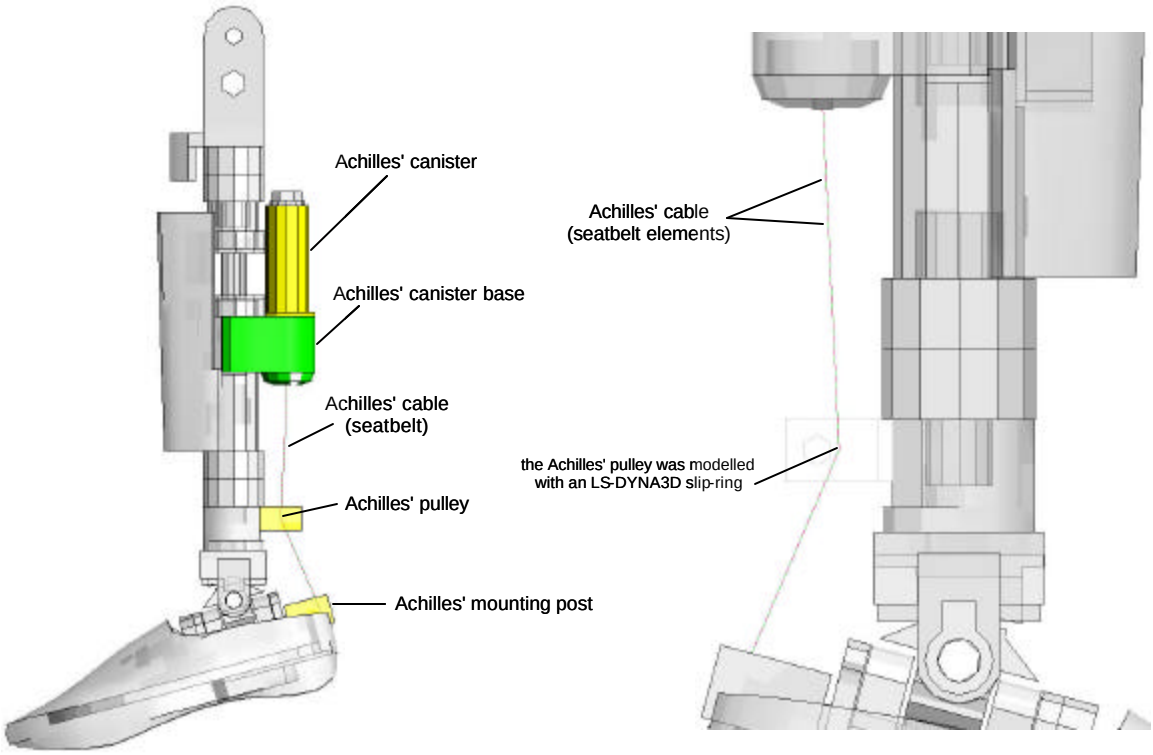

Figure 10: Modeling of the Achilles' cable in the THOR-LX.

MODEL OUTPUT

The THOR-LX FE model has been designed to output the same measurements reported by the physical THOR-LX dummy. In order to ensure proper processing of the output data, the following information is provided on model conventions, definitions, polarities, and output files.

Conventions and Numbering

The units used in the THOR-LX FE model are: mass in metric tons (10^3 kg), length in millimeters, and time in seconds. The origin point (0, 0, 0) of the global coordinate system is located at the THOR H-Point, as shown in Figure 11. The positive global X-axis points towards the anterior end of THOR. The positive global Y-axis points towards the right lateral end of THOR. The positive global Z-axis points towards the inferior end of THOR. There are local coordinate systems in the FE model of THOR-LX to maintain local output for the two load-cells, the ankle joints, and the two accelerometers. The local coordinate systems are attached to the FE model using *DEFINE_COORDINATE_NODES. There is one vector defined in the model (*DEFINE_SD_ORIENTATION) that follows the tibia compliance spring to maintain the local output for compression and the force passing through that spring. The lower numbering index in the left THOR-LX FE model starts at 500,001.

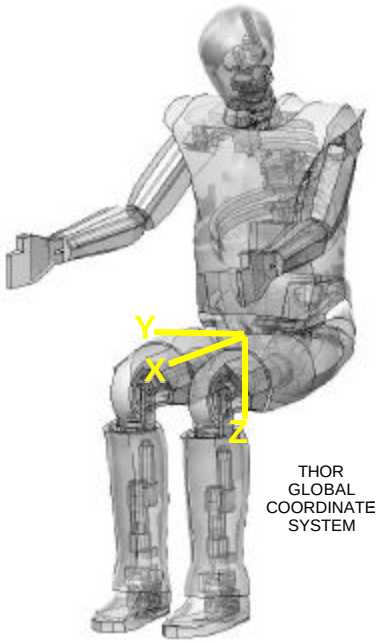

Figure 11. The THOR-LX FE model global coordinate system.

Data Acquisition and Model Output

The data acquisition in the physical THOR-LX includes two load-cells, three potentiometers, and two accelerometers. The location of these devices in the THOR-LX FE model is shown in Figure 12. The THOR-LX has a lower and an upper tibia load-

cell, the upper load cell monitors Fx, Fz, Mx, and My while the lower monitors Fx, Fy, Fz, Mx, and My. In the finite element model, the two load-cells are implemented using *CONSTRAINED_JOINT_LOCKING_LOCAL. Each physical load-cell was split into two parts in the FE model in order to define the locking joints. The output for the forces in the load cell can be found in the *jntforc* ASCII file. Potentiometers record the rotation angles in the physical ankle joint. In the FE model, the output for the rotation angles and the angular velocities in the ankle is implemented through the definition of *CONSTRAINED_JOINT_STIFFNESS_GENERALIZED and can also be found in the *jntforc* ASCII file.

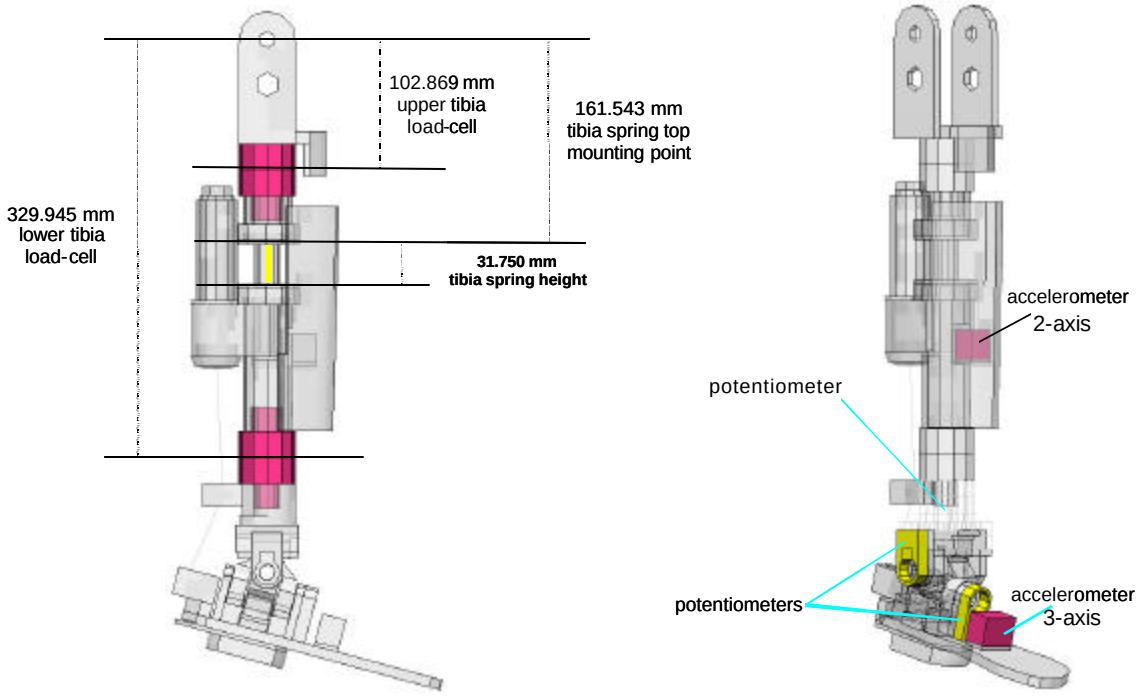

Figure 12. Locations of the THOR-LX data acquisition devices.

THOR-LX has a tibia mid anterior accelerometer measuring Ax and Ay (using two uniaxial accelerometers) and a mid-foot accelerometer measuring Ax, Ay, and Az (using either three uniaxial accelerometers or one triaxial accelerometer). In the FE model, the output acceleration signal at the accelerometer locations is implemented through the definition of *DATABASE_HISTORY_NODE_LOCAL which outputs the information to the *nodout* ASCII file. In addition to the accelerometers, the *nodout* file also contains data recorded to monitor the output of: the contoured foot compression, the tibia spring compression, and the Achilles' cable. The user should review the following ASCII

output: *deforc* - for the tibia spring loads and *sbtout* - for the Achilles' cable loads. Table 2 provides a list of each component in the data acquisition with the corresponding output file, node, or joint number, and the necessary polarity change to replicate the output from the physical THOR-LX. It is also recommended that the user review all available ASCII output, including the *glstat* and *matsum* for energy balance.

Table 2. Output files used to replicate the THOR-LX data acquisition. (Note: using pre-processors like Hypermesh can change the order of the joint definitions which may change the Joint ID #s listed below).

Data Source	Node / Joint ID	Output File
Lower Tibia Load Cell	1	jntforc
Upper Tibia Load Cell	2	jntforc
Tibia Compression Trans Joint	3	jntforc
Dorsi / Plantar Joint Rotation	4	jntforc
Eversion/ Inversion Joint Rotation	5	jntforc
Internal/External Joint Rotation	6	jntforc
Tibia Accelerometer	501556	nodout
Foot Accelerometer	505687	nodout
Achilles Force	N/A	sbtout
Tibia Compression	507005, 507003	nodout

MODEL CORRELATION

Simulations were performed with the THOR-LX FE model to ensure that the model has a similar behavior to the physical THOR-LX. The run time for most of the simulations was 120 ms, which took about 15 minutes on a 2.5 GHz PC. Data from tests of the physical THOR-LX used for comparison was provided by Vehicle Research and Test Center (VRTC). The test and simulation procedures are described below, as well as the process for data acquisition.

Test Descriptions

The tests used to evaluate the FE model performance were:

- Three ball impact tests to evaluate the dorsi joint performance
- Two heel impact tests to evaluate the tibia compliance
- Three Achilles' tests to evaluate the Achilles' cable
- Two skin tests to assess the effect of the skin on the model.

Gravity was not considered in THOR-LX FE correlation simulations. A pendulum type impactor with a 63.5 mm diameter and a 5.00 kg mass was introduced in the correlation models.

The ball impact tests were conducted with the foot in the neutral position (Figure 13). In each test the impactor struck the ball of the foot 102.5 mm anterior of the dorsi-plantar joint. There was no leg-skin for these tests, as this part was removed during lab testing. In the first ball impact test, the impactor speed was 5 m/s and the test set-up used a full THOR-LX with the upper tibia replaced by a single cylinder that was fixed in all directions. In the simulation, the translational joint and load cell at the upper tibia were removed, making the tibia rigid. The impactor initial velocity in the second and third ball impact tests was 3.17 m/s. The second ball impact test used a complete THOR-LX with the Achilles' cable was removed (in both the test and simulation). The third ball impact used an intact THOR-LX without any modification.

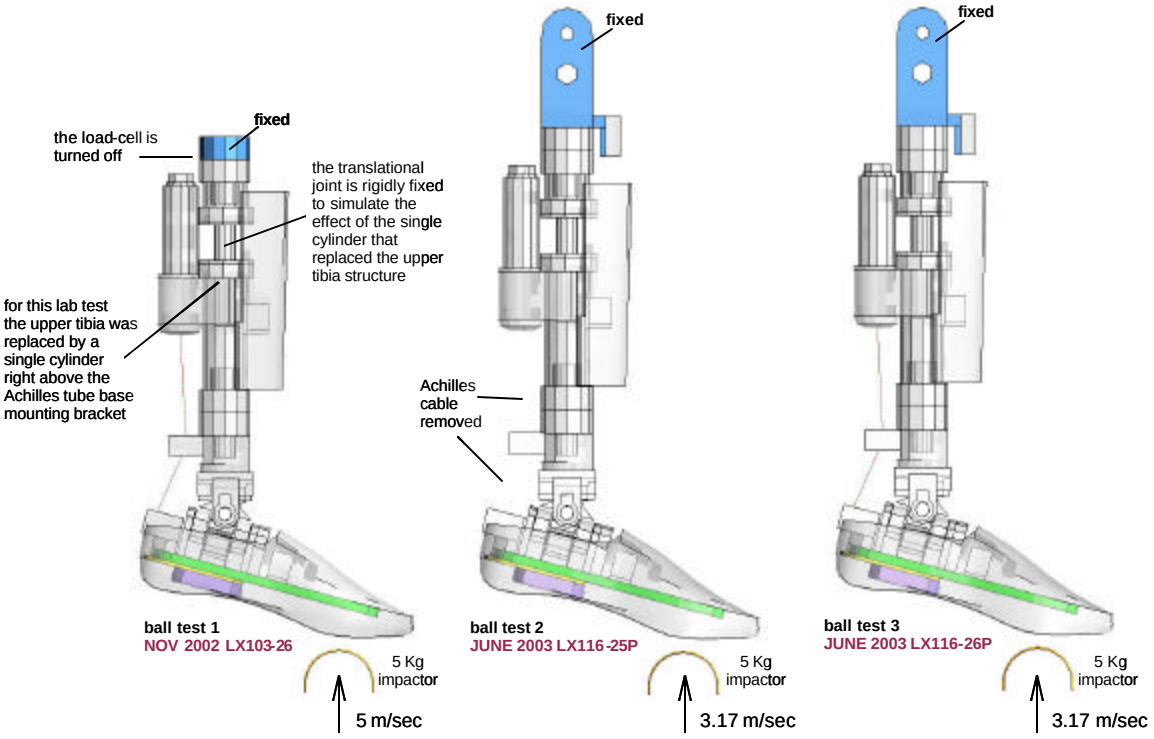

Figure 13. Setup and modification for specific ball impact tests.

The heel impact tests were conducted with the foot in the horizontal position and used the complete THOR-LX (Figures 14 and 15). Again, the leg-skin was removed during lab

testing. Before the simulations, the foot was rotated from 15 degrees of plantar flexion to the horizontal position and the Achilles' cable was adjusted to match the test conditions. The center of the impactor in each test was aligned with the center of the dorsi-plantar joint, as shown in Figure 14. In the first heel impact test, the impactor had an initial velocity of 5 m/s and the dorsi joint was restricted from rotating with duct tape. The second heel impact test used an impactor speed of 3.97 m/s and had a metal bracket to restrict motion in the dorsi joint. Both tests were simulated by locking the motion at the dorsi joint.

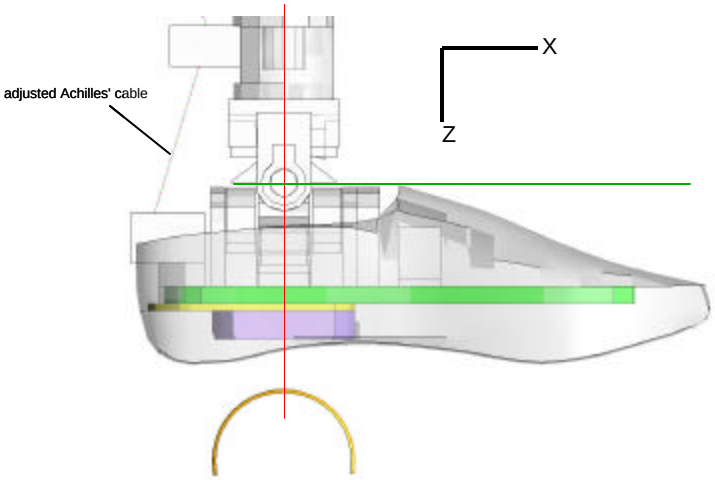

Figure 14. General heel impact test setup.

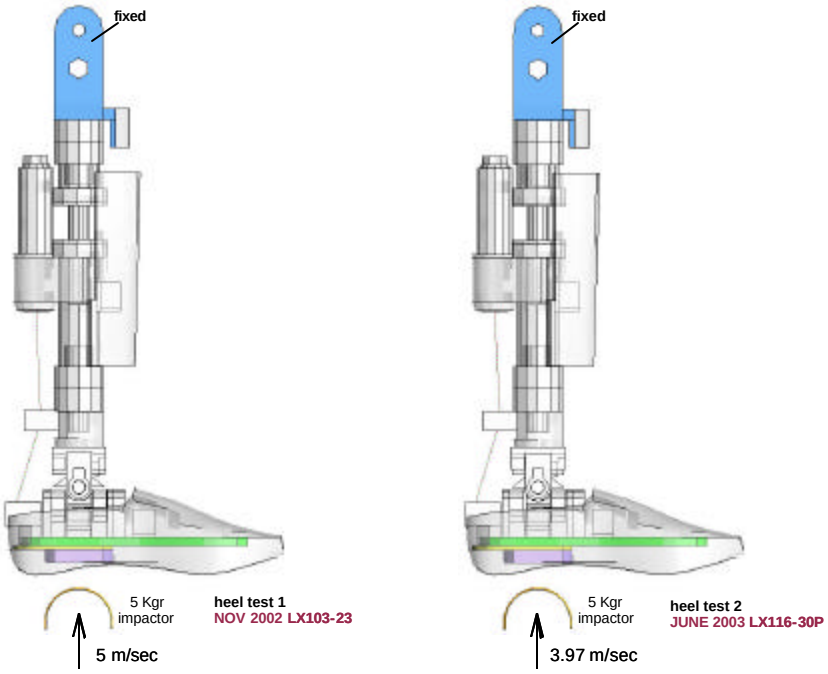

Figure 15. Setup for specific heel impact tests.

Each of the Achilles' tests used a similar setup to the ball impact tests. However, the experimental tests included an Achilles' load cell that allowed a direct comparison between the simulation and the experiment. Also, the impactor in the Achilles' tests was 8.3 kg and had a diameter of 76.2 mm. The impactor velocity for each of the Achilles' tests was 3.1 m/s, 3.9 m/s, and 4.3 m/s for tests 1, 2, and 3 respectively.

The two skin tests used the same setup as the heel impact tests, including both velocities and impactors. Experimental data only exists for the 5 m/s case but both simulations are shown. This is done to offer a comparison between the skin and no skin cases within the simulations as well.

Data Acquisition Procedures

There was no direct recording of the dorsi moment in the lab tests. Yet, there was a need to calculate the test moment at the dorsi joint, for the purpose of correlating between the test and the FE model. The moment, My, and force, Fx, at the lower tibia load cell, as well as the loads in the Achilles' cable, were used for that purpose, as shown in the free body diagram (Figure 16). In ball tests 1 and 3, the Achilles' cable loads were not recorded during testing in the lab. So, a manual calculation of the dorsi moment based on the test output was only possible for the second ball test where Achilles' cable was not present in the experimental apparatus. In that case only, the test dorsi moment is given as:

$$M_{dorsi} = -My - Fx.H$$

For ball tests 1 and 3, the test moment on the dorsi joint can only be used as a rough estimate since the calculation is not exact, due to a lack of test information on the Achilles' cable force.

In the heel impact tests, the tibia bushing compression was only measured in the first heel impact test and was calculated later from video of the test. When results from the FE model were compared with the lab results, similar methods were used to ensure compatibility.

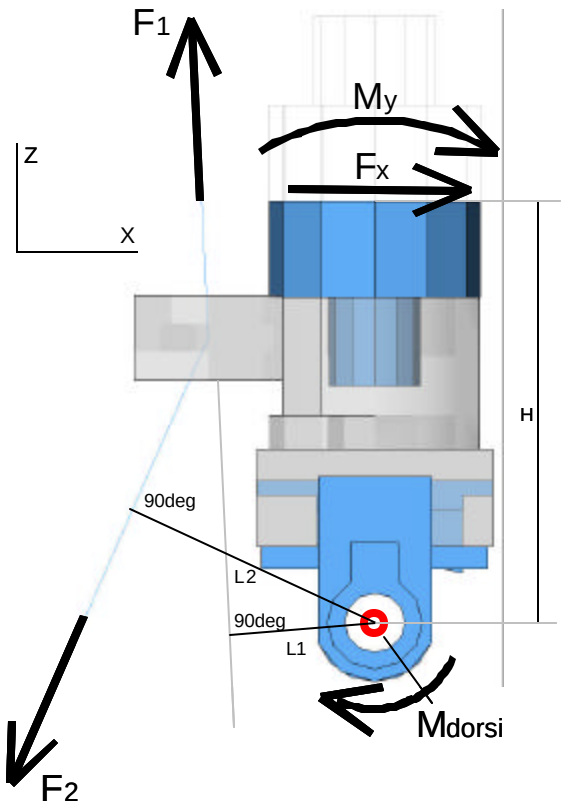

Figure 16. Balance of moments about the dorsi joint.

Results Summary

The results for each of the tests are presented in Appendix I. Charts are provided that compare the experimental results to those in the simulations. The results from the computer model are labeled "Simulation" and the lab test results are labeled "Experiment." All of the data from the simulations was resampled at 10000 Hz. This was necessary because the LS-DYNA simulations did not have a constant time step. The data was then filtered with a CFC 60 (100 Hz) Butterworth 4 pole filter to avoid phase shifts. Some of the polarities for the simulation curves were reversed to match the conventions used for the experimental tests. For the ball impact tests, results are provided for

impactor deceleration, ankle joint motion, and load cell data. Results for the heel tests include impactor deceleration, and load cell data. (Tibia compression data is available for heel test one only.) The Achilles' tests show a comparison of the Achilles' force. This is due to the lack of availability of other test data. The skin tests show tibia compression and tibia forces, since these measurements are most likely to be affected by the skin.

In general, all of the ball and heel simulations match the experimental results very well, thus showing that the finite element model is a good representation of the physical THOR-LX. The Achilles' tests show that the Achilles' force in the simulation follows the trend seen in the experiments. However, these results do not show any effects of hysteresis. Hysteresis may be added in future versions of the THOR-LX FE model. The model results for the skin tests show that there is a slight reduction in tibia force and compression when the skin is included, as seen in the experiments.

CONCLUSIONS

A finite element model was developed to represent the response of the THOR-LX (THOR lower extremity). The model provides a realistic geometric and material representation of most parts of the physical THOR-LX. Deformable parts were modeled using a variety of techniques that accurately represent the physical model. A fully functional ankle has been defined using mathematical stiffness and damping responses that correspond to the physical THOR-LX ankle. Instructions have been provided on how to output the same measurements from the FE model that are found in the physical THOR-LX data acquisition. Finally, results have been presented that show the correlation of the finite element model with the physical THOR-LX. The THOR-LX FE model can be used as a computational tool that predicts the results of a physical test with the THOR-LX.

ACKNOWLEDGMENTS

The authors would like to thank Dan Rhule from the Vehicle Research and Test Center (VRTC), Tariq Shams from GESAC, and Rolf Eppinger, Erik Takhounts, and Mark Haffner from the US Department of Transportation.

REFERENCES

1. Certification Procedure For The Thor-Lx/Hybrid III Retrofit Version 3.2 (2001) National Highway Traffic Safety Administration Vehicle Research and Test Center, link on 2/2/04 http://www-nrd.nhtsa.dot.gov/pdf/nrd-51/MiscBio/LX_CertProc32.pdf
2. Kwok, P., Yu, H., Medri, M., Zhou, Q. Validation of Finite Element Model of THOR Lower Leg. (2001) Vehicle Crashworthiness Division, DTS-74. Volpe National Transportation Systems Center, Cambridge, Massachusetts.
3. Shams, T., Beach, D., White, R.P., Rangarajan, N., Haffner, M., Eppinger, R., Pritz, H., Kuppa, S., Beebe, M. (1999) Development and Design of Thor-Lx: The Thor Lower Extremity. Proc. 43rd Stapp Car Crash Conference.
4. THOR-LX User's Manual Version 3.2 (2001), link on 2/2/04 http://www-nrd.nhtsa.dot.gov/departments/nrd-51/thor_lx/LX_manual.html
5. Zhou, Q., Yu, H., Medri, M. B., and DiMasi, F., Finite element model of THOR dummy lower leg, 2002 ASME International Mechanical Engineering Congress & Exposition, IMECE2002-39171, New Orleans, Louisiana, November 17-22, 2002.

APPENDIX I

Ball Impact Test 1

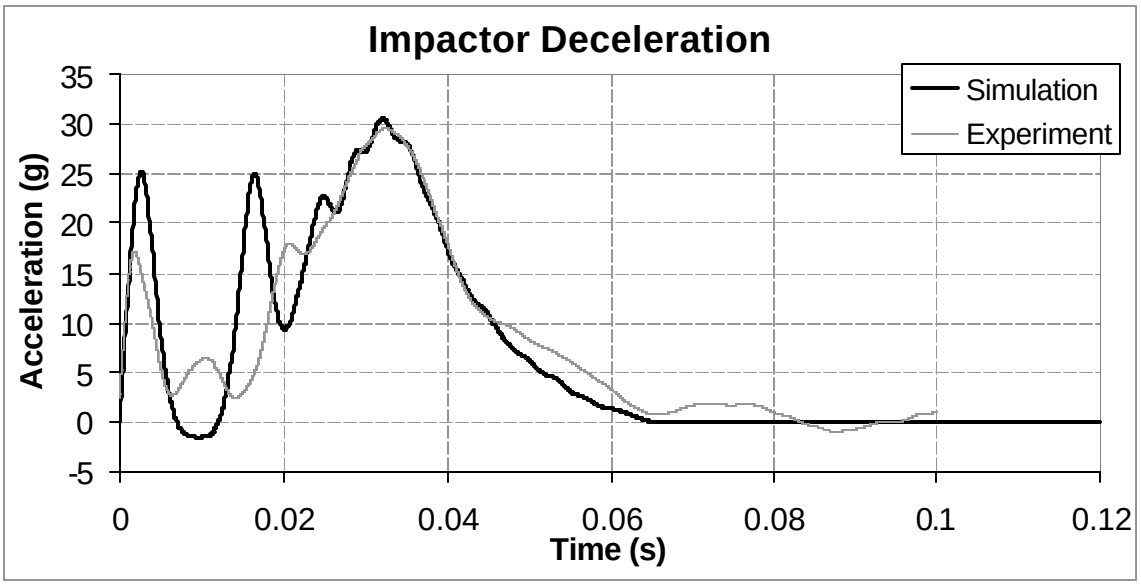

Figure 17. Ball Test 1: Impactor deceleration.

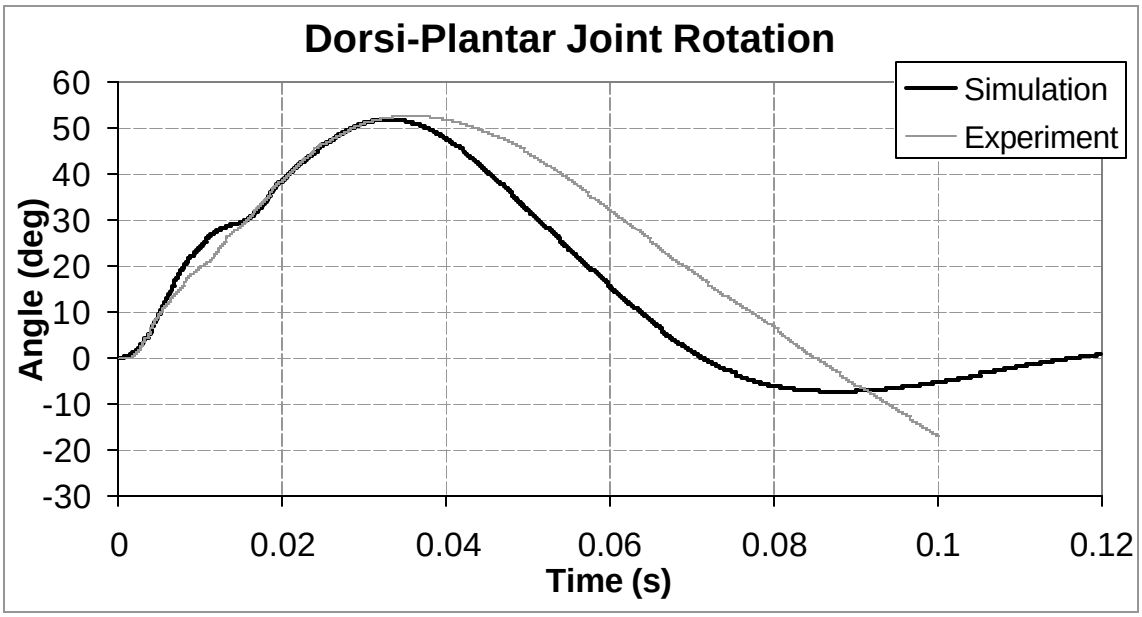

Figure 18. Ball Test 1: Dorsi-plantar joint rotation.

Note: All of the data from the simulations were resampled at 1000 Hz and then filtered with a CFC 60 (100 Hz) Butterworth 4 pole filter.

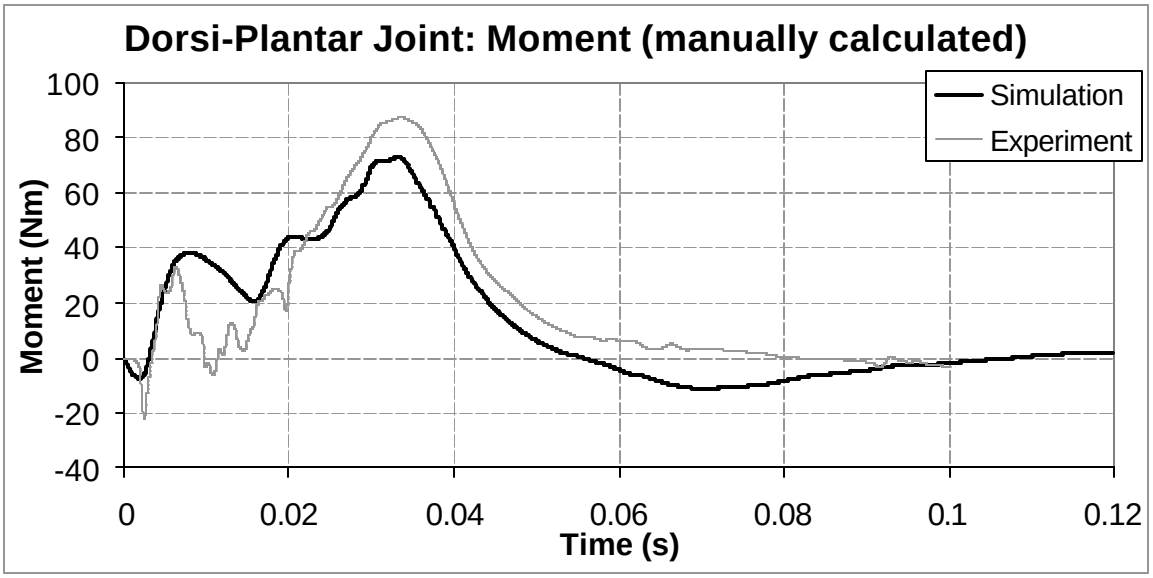

Figure 19. Ball Test 1: Dorsi-plantar joint moment, no Achilles contribution.

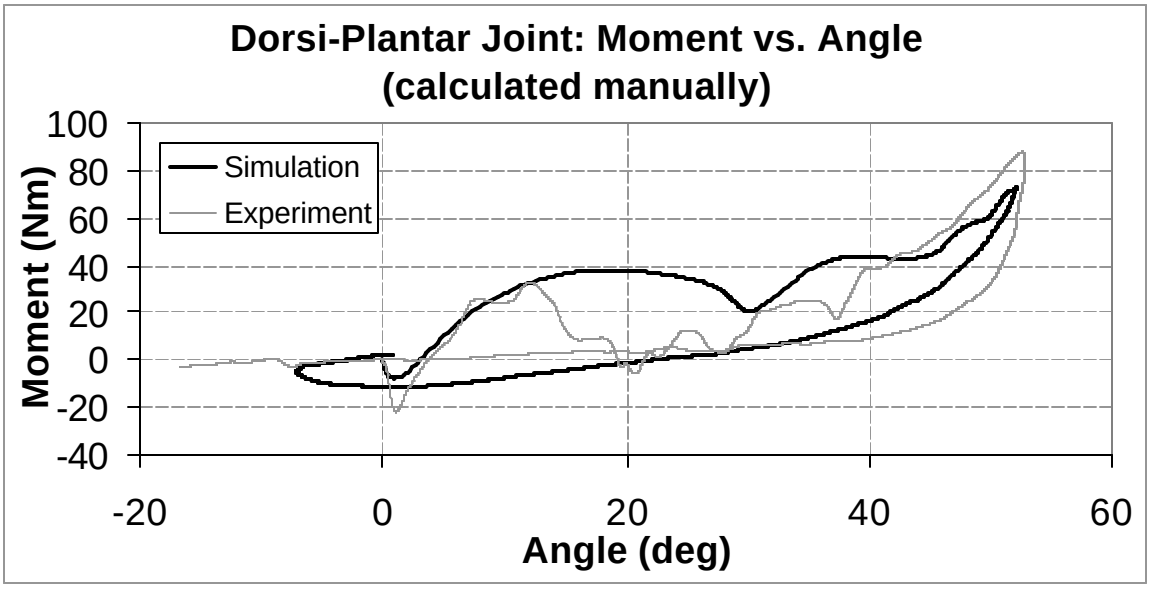

Figure 20. Ball Test 1: Dorsi-plantar joint moment vs. angle, no Achilles contribution.

Note: All of the data from the simulations were resampled at 1000 Hz and then filtered with a CFC 60 (100 Hz) Butterworth 4 pole filter.

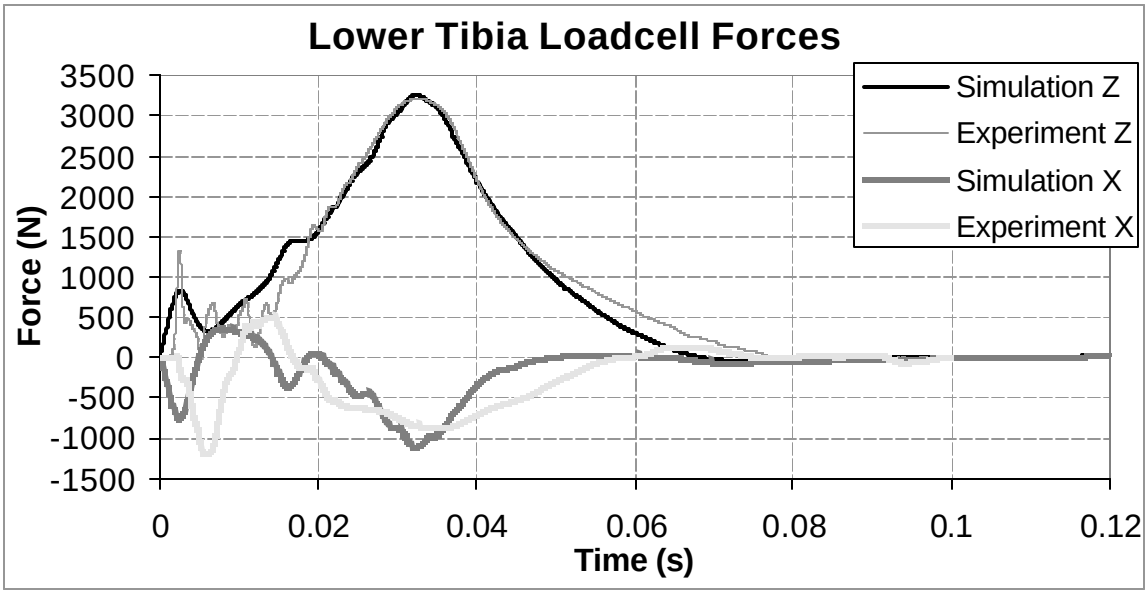

Figure 21. Ball Test 1: Lower tibia load cell forces.

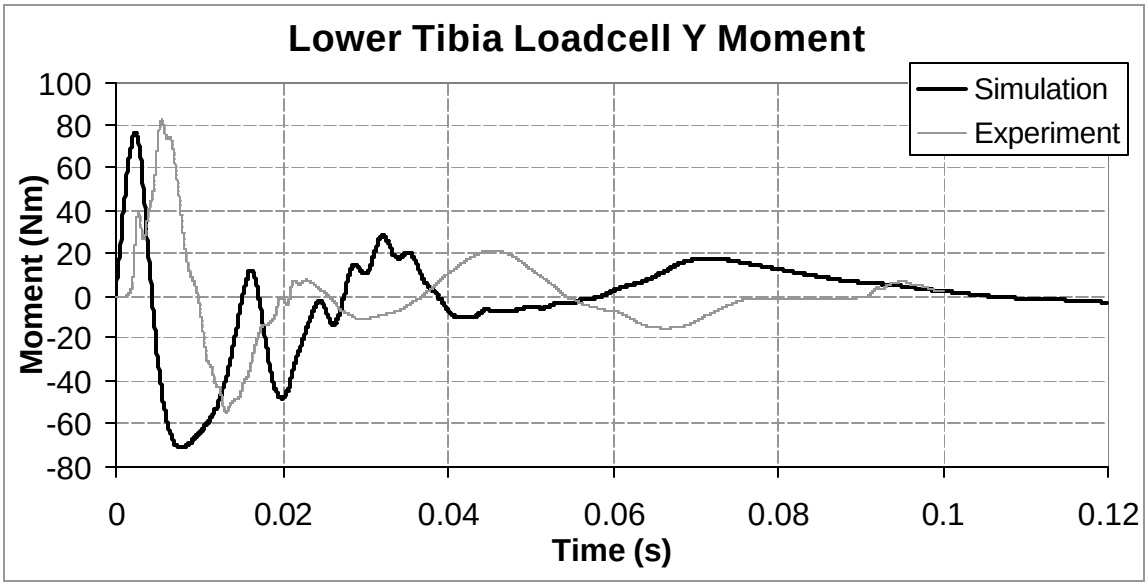

Figure 22. Ball Test 1: Lower tibia load cell moments.

Note: All of the data from the simulations were resampled at 1000 Hz and then filtered with a CFC 60 (100 Hz) Butterworth 4 pole filter.

Ball Impact Test 2

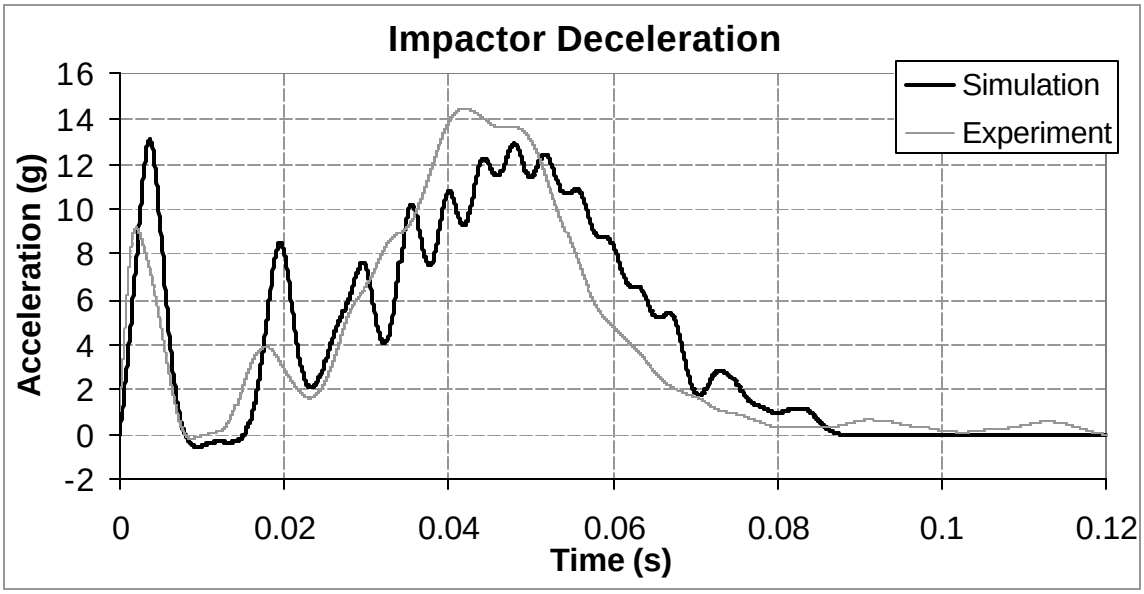

Figure 23. Ball Test 2: Impactor deceleration.

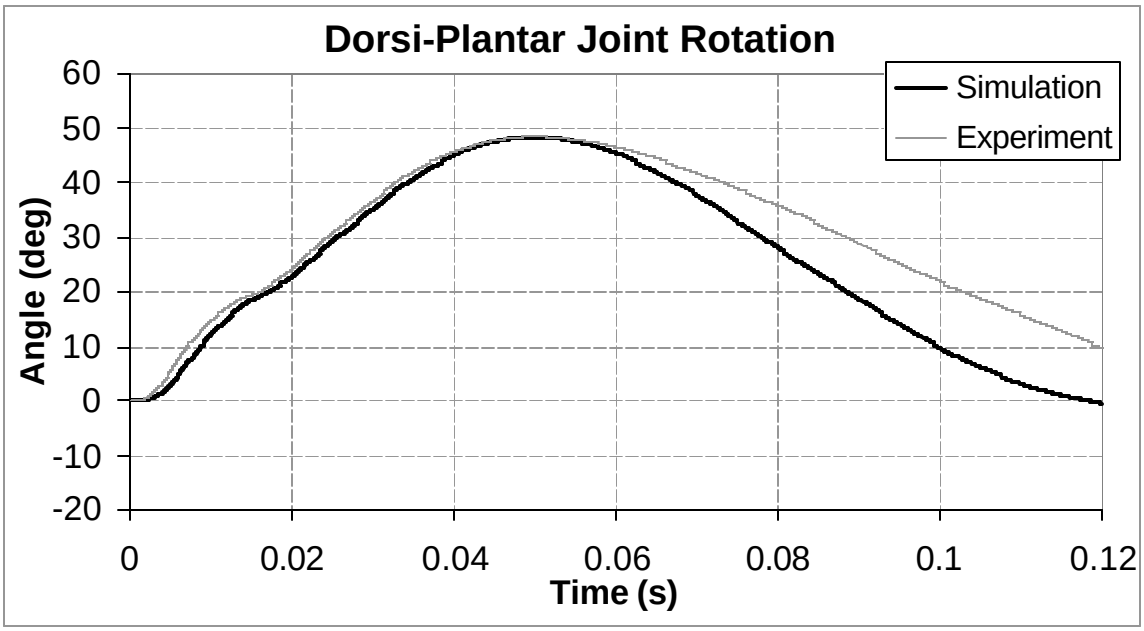

Figure 24. Ball Test 2: Dorsi-plantar joint rotation.

Note: All of the data from the simulations were resampled at 1000 Hz and then filtered with a CFC 60 (100 Hz) Butterworth 4 pole filter.

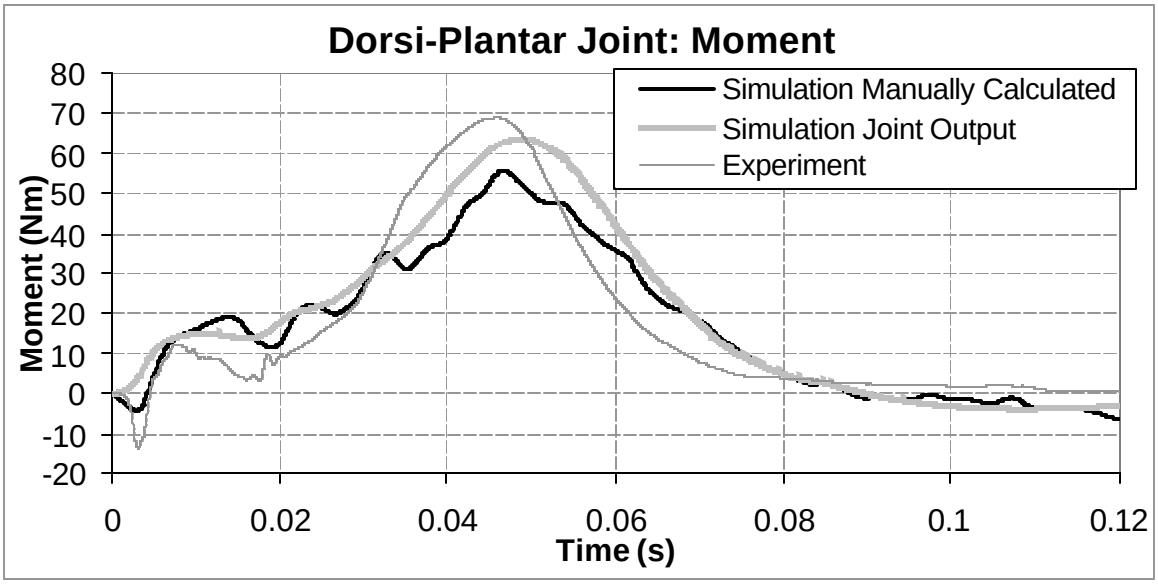

Figure 25. Ball Test 2: Dorsi-plantar joint moment.

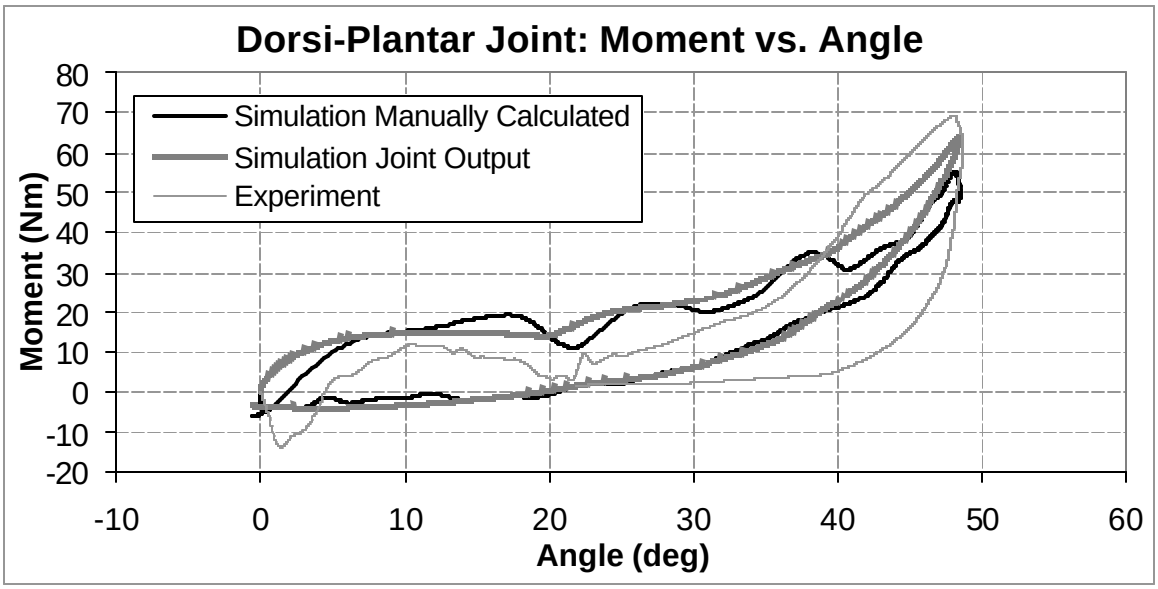

Figure 26. Ball Test 2: Dorsi-plantar joint moment vs. angle.

Note: All of the data from the simulations were resampled at 1000 Hz and then filtered with a CFC 60 (100 Hz) Butterworth 4 pole filter.

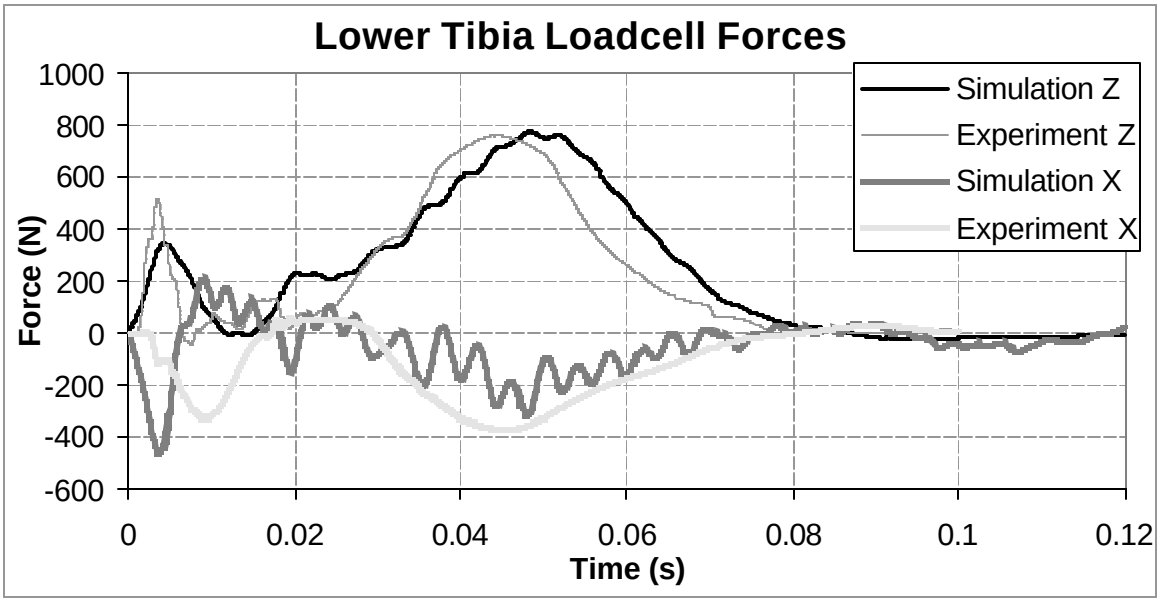

Figure 27. Ball Test 2: Lower tibia load cell forces.

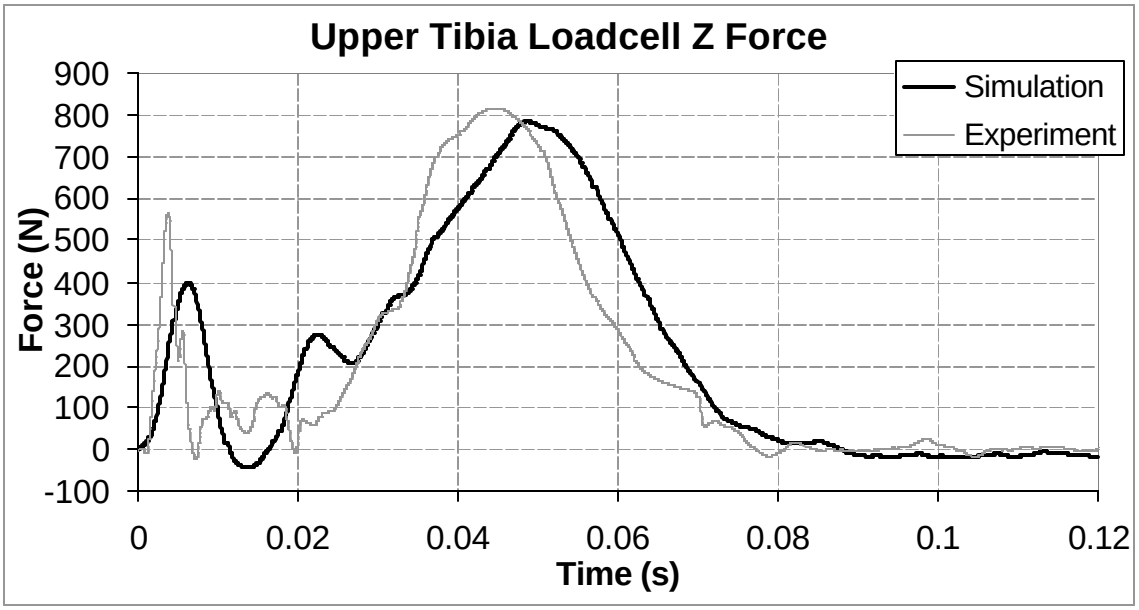

Figure 28. Ball Test 2: Upper tibia load cell forces.

Note: All of the data from the simulations were resampled at 1000 Hz and then filtered with a CFC 60 (100 Hz) Butterworth 4 pole filter.

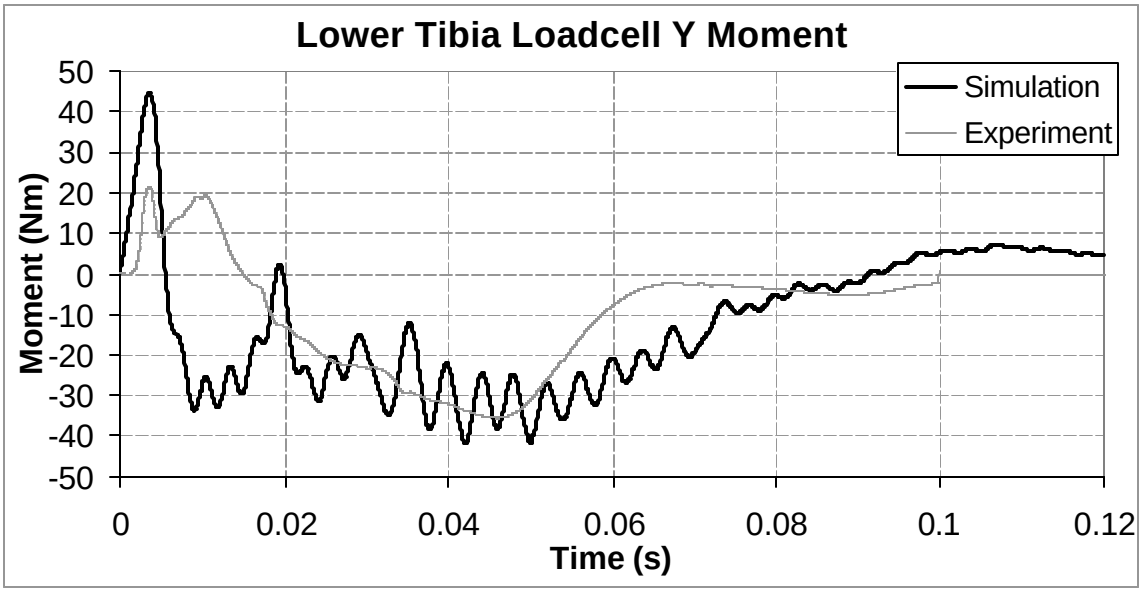

Figure 29. Ball Test 2: Lower tibia load cell moments.

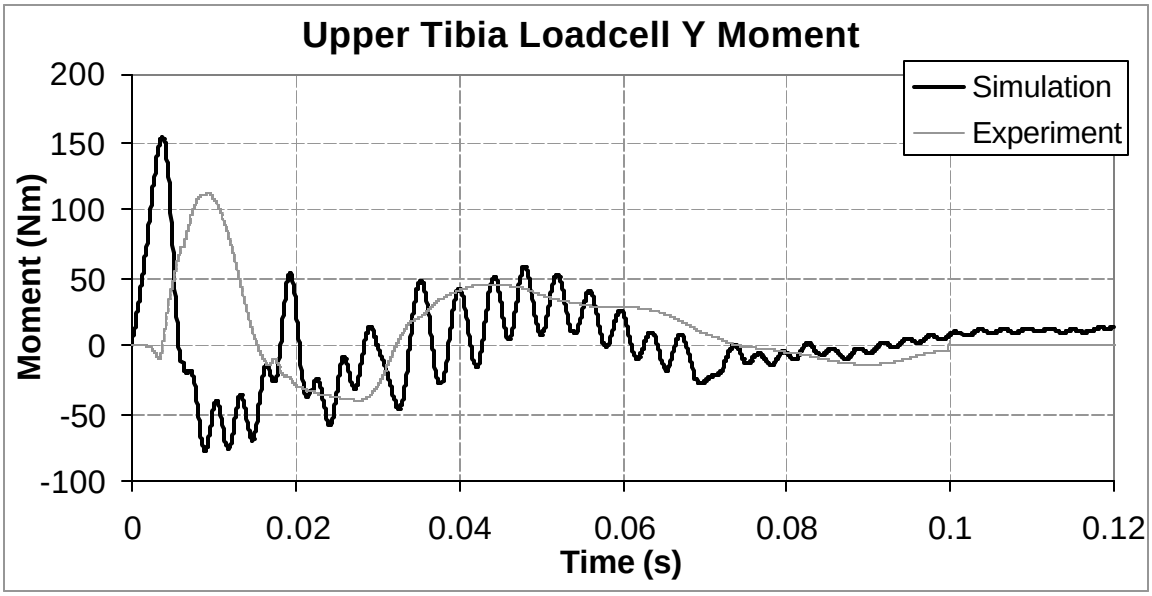

Figure 30. Ball Test 2: Upper tibia load cell moments.

Note: All of the data from the simulations were resampled at 1000 Hz and then filtered with a CFC 60 (100 Hz) Butterworth 4 pole filter.

Ball Impact Test 3

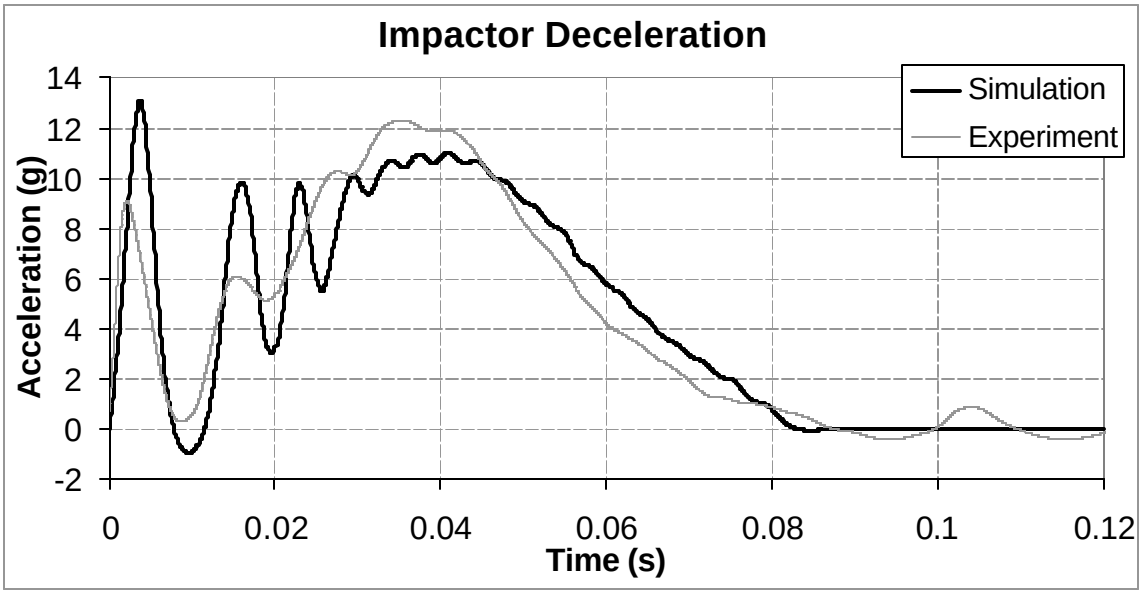

Figure 31. Ball Test 3: Impactor deceleration.

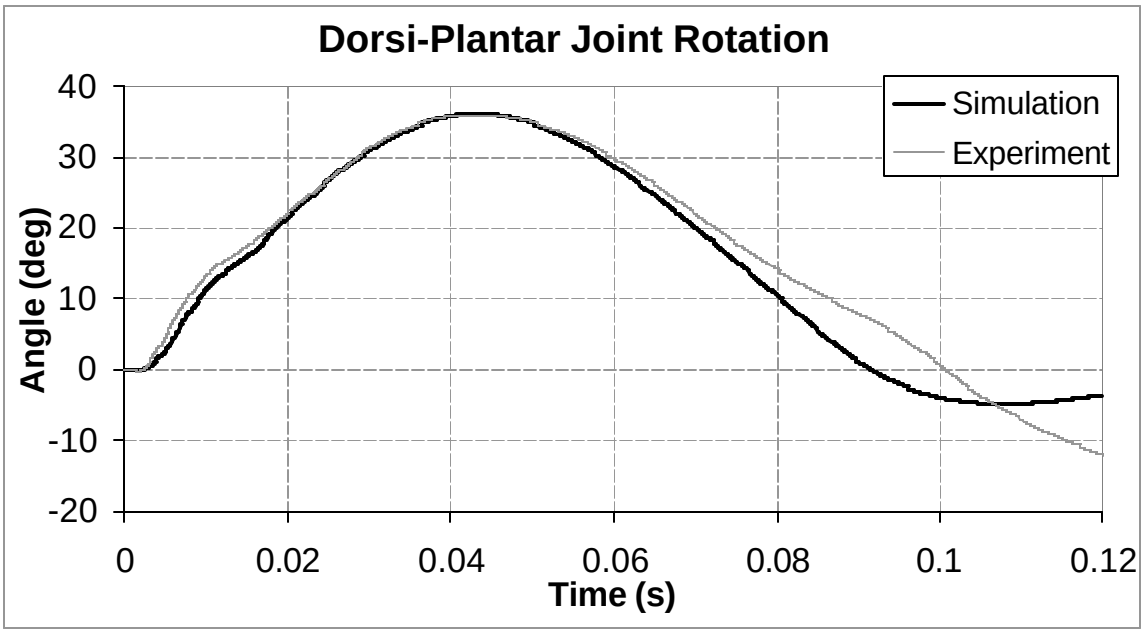

Figure 32. Ball Test 3: Dorsi-plantar joint rotation.

Note: All of the data from the simulations were resampled at 1000 Hz and then filtered with a CFC 60 (100 Hz) Butterworth 4 pole filter.

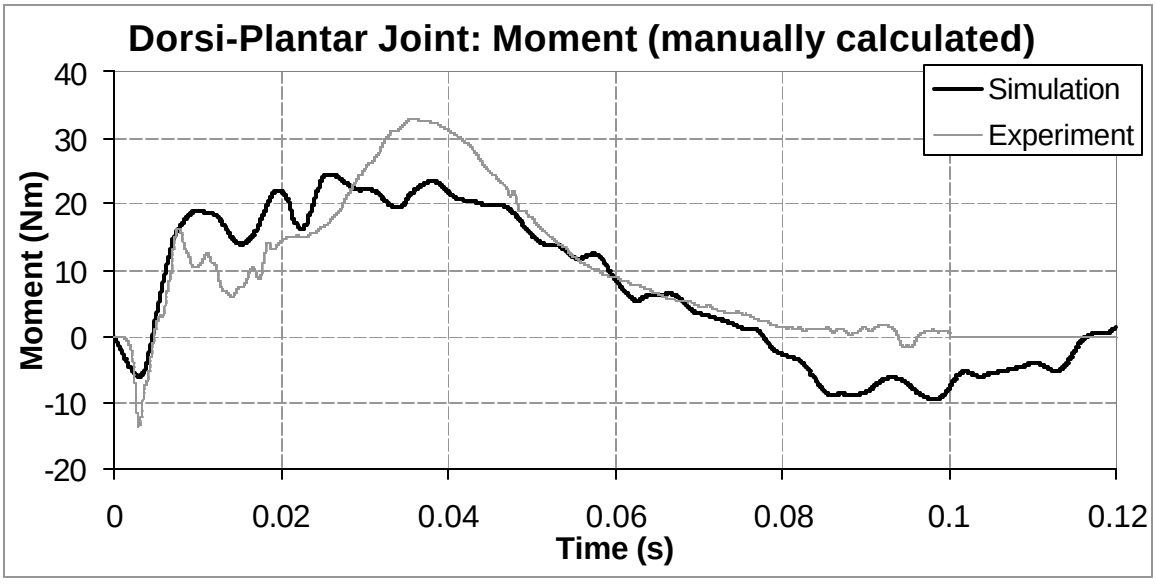

Figure 33. Ball Test 3: Dorsi-plantar joint moment, no Achilles contribution.

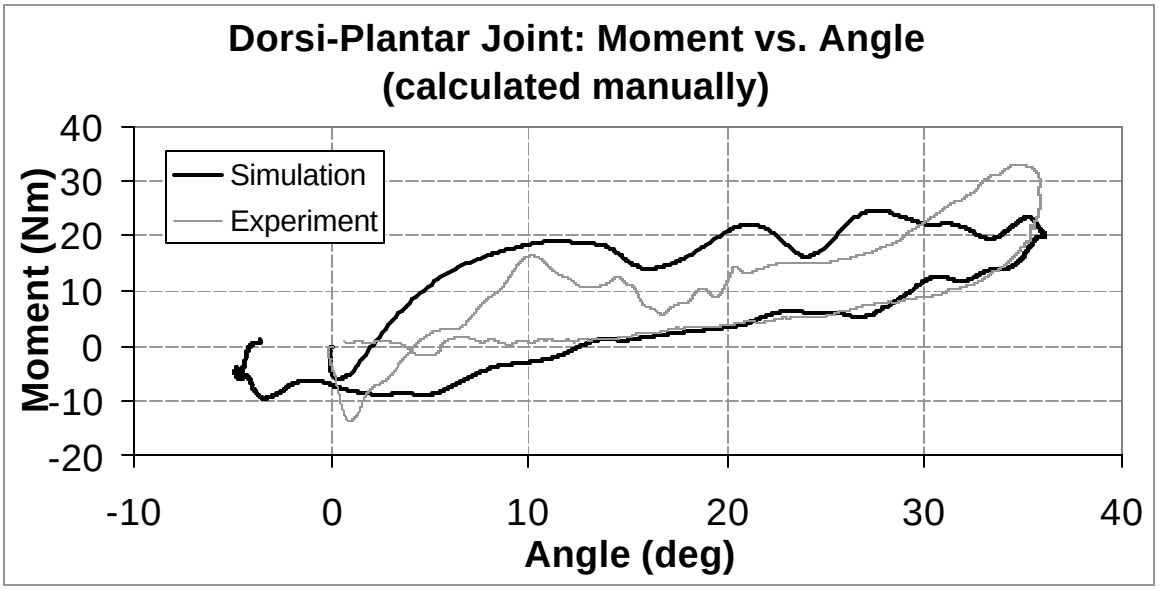

Figure 34. Ball Test 3: Dorsi-plantar joint moment vs. angle, no Achilles contribution.

Note: All of the data from the simulations were resampled at 1000 Hz and then filtered with a CFC 60 (100 Hz) Butterworth 4 pole filter.

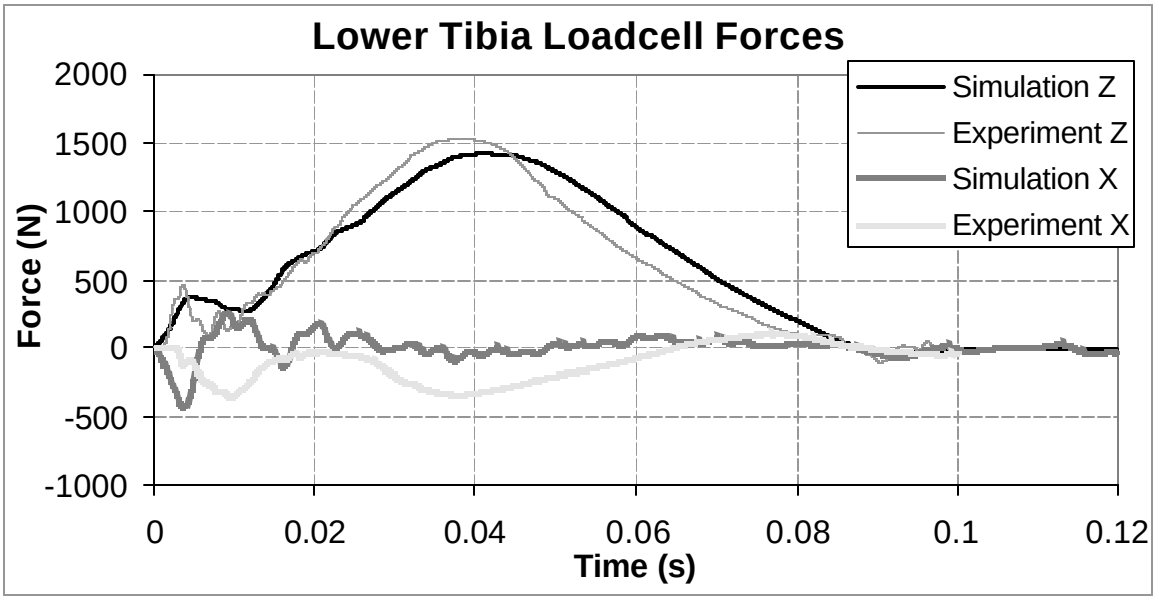

Figure 35. Ball Test 3: Lower tibia load cell forces.

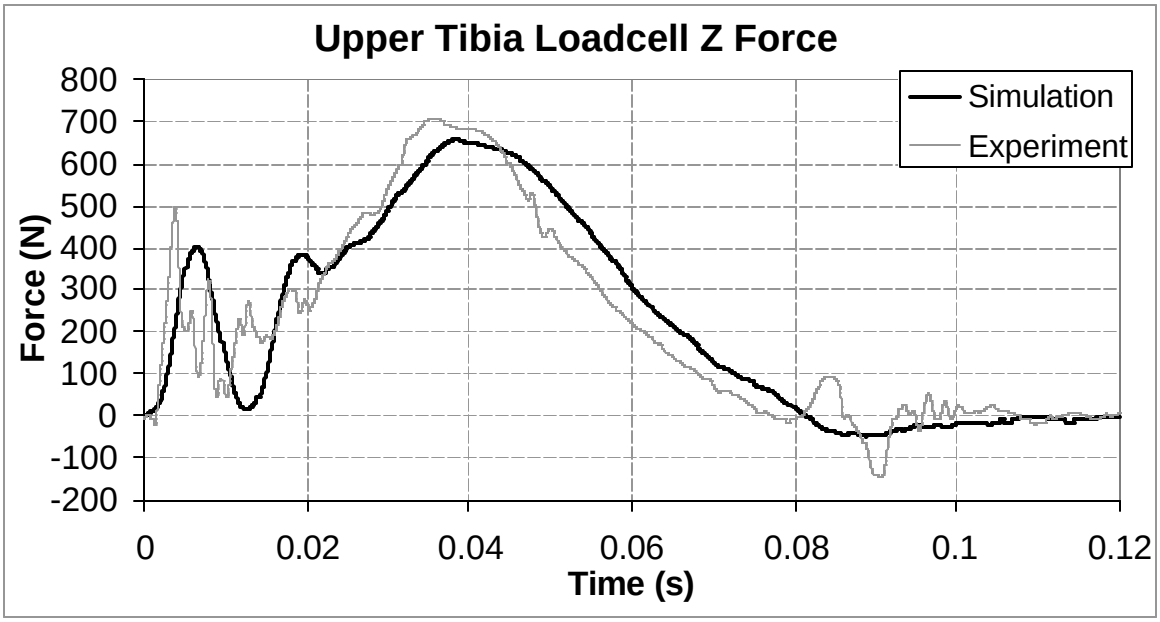

Figure 36. Ball Test 3: Upper tibia load cell forces.

Note: All of the data from the simulations were resampled at 1000 Hz and then filtered with a CFC 60 (100 Hz) Butterworth 4 pole filter.

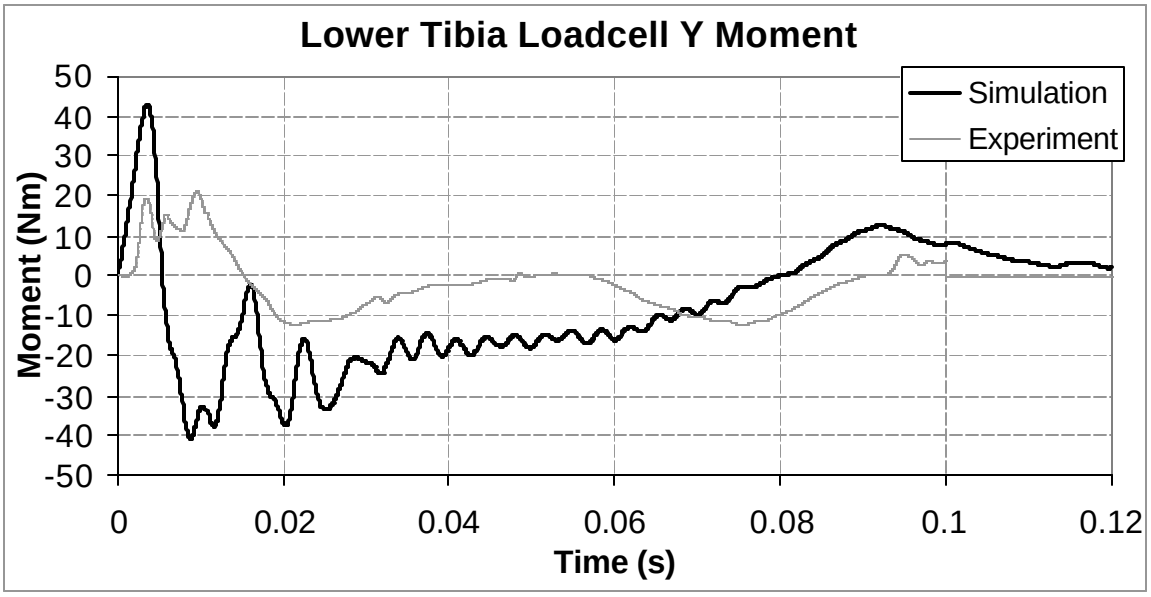

Figure 37. Ball Test 3: Lower tibia load cell moments.

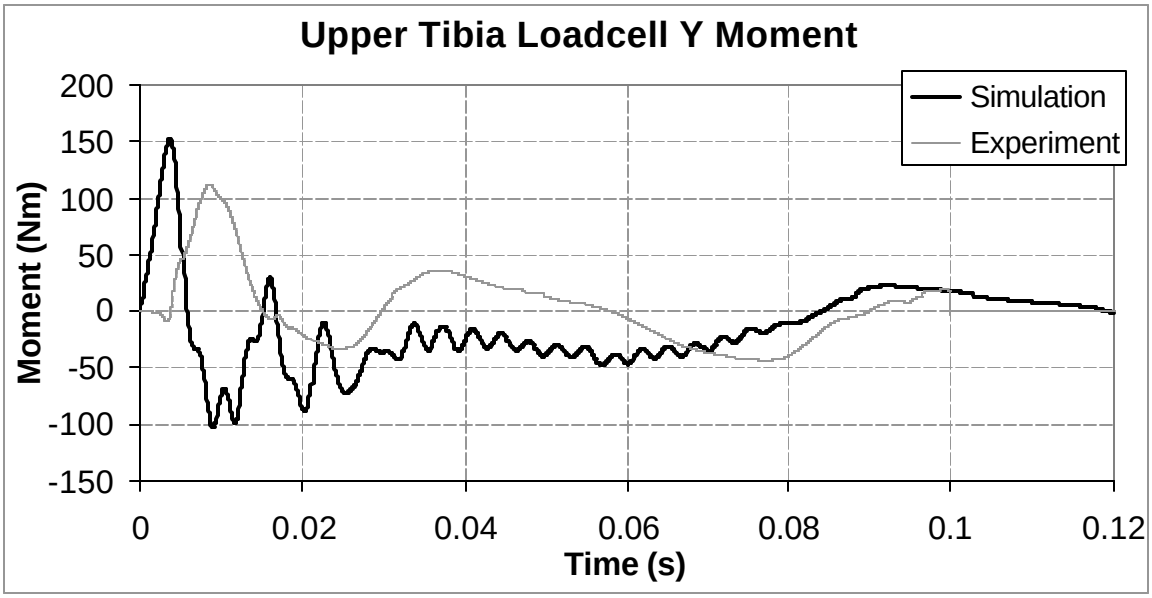

Figure 38. Ball Test 3: Upper tibia load cell moments.

Note: All of the data from the simulations were resampled at 1000 Hz and then filtered with a CFC 60 (100 Hz) Butterworth 4 pole filter.

Heel Impact Test 1

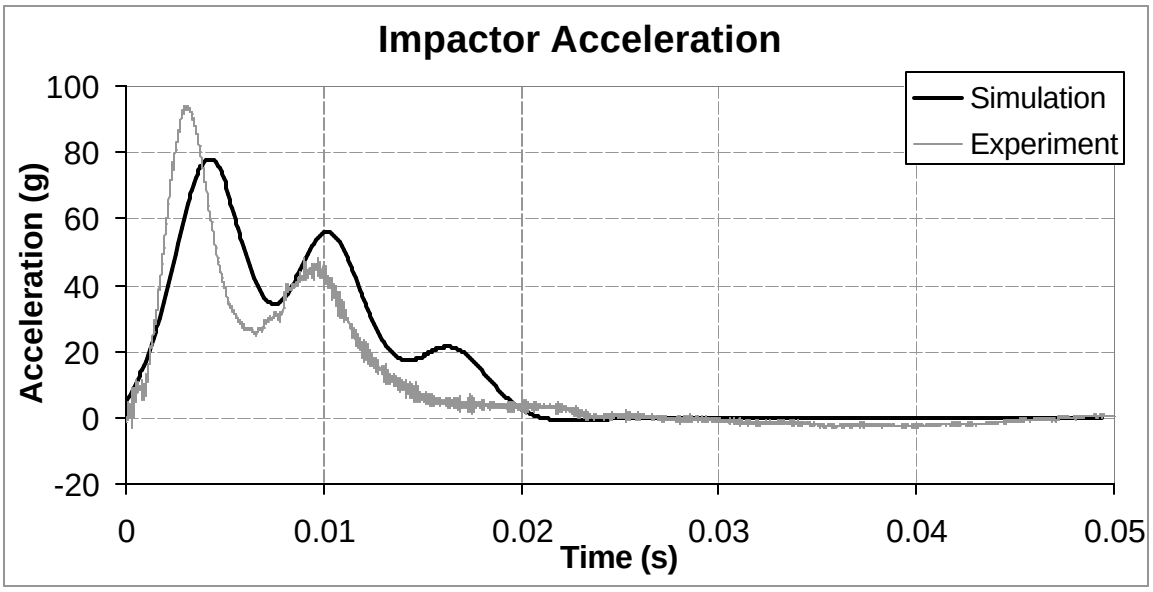

Figure 39. Heel Test 1: Impactor deceleration.

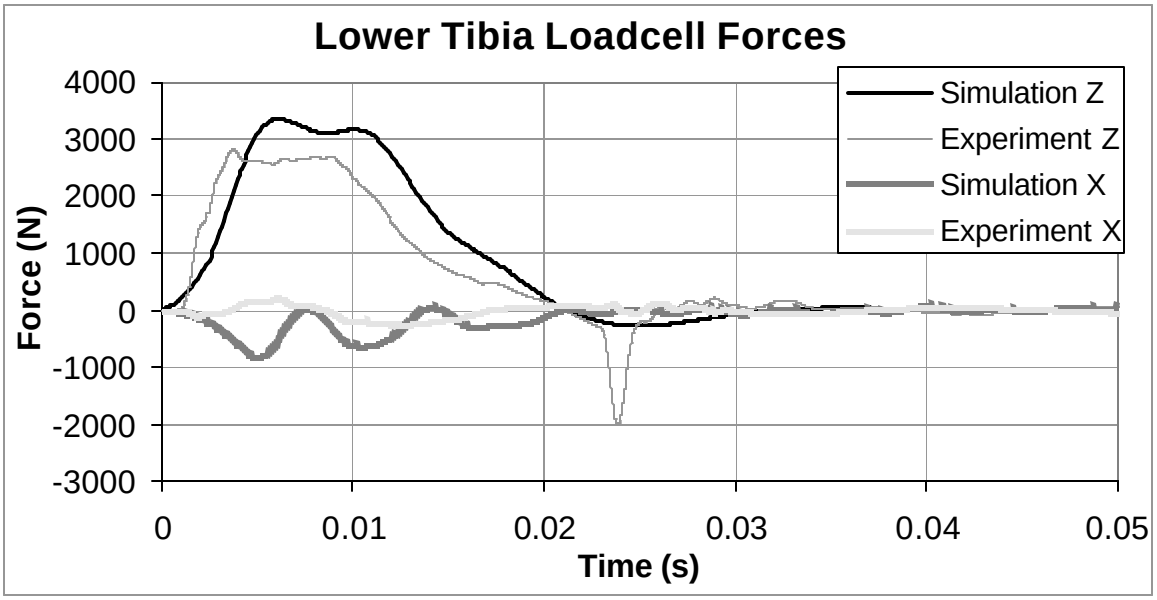

Figure 40. Heel Test 1: Lower tibia load cell forces.*

*The source of this rebound artifact has been identified, and is currently being addressed in the physical THOR-Lx design. The model is correct in not reproducing this artifact.

Note: All of the data from the simulations were resampled at 1000 Hz and then filtered with a CFC 60 (100 Hz) Butterworth 4 pole filter.

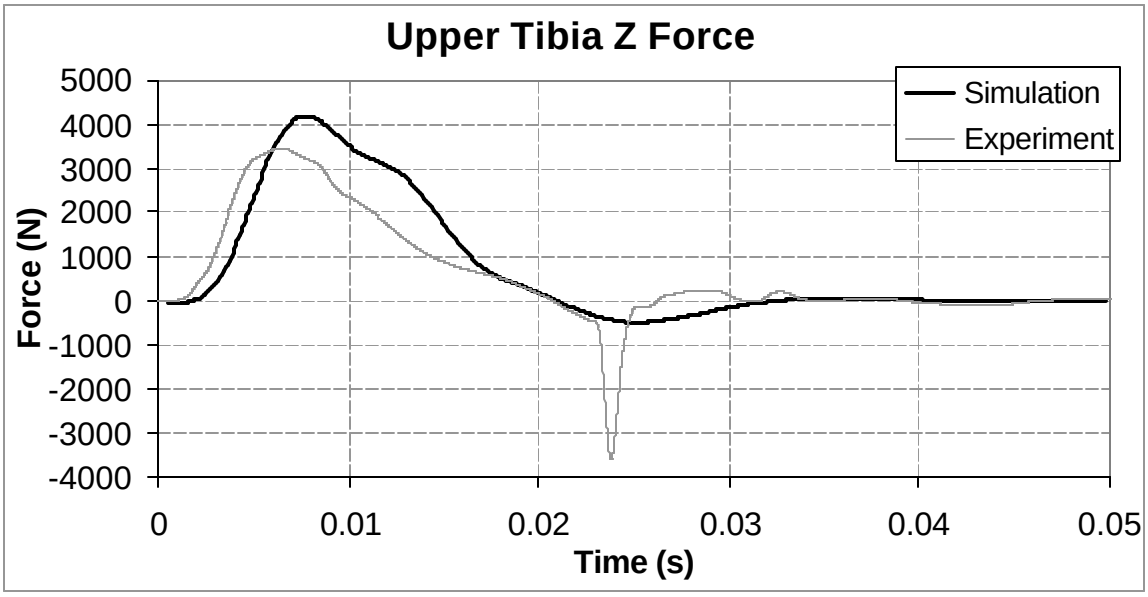

Figure 41. Heel Test 1: Upper tibia load cell forces.*

Heel Impact Test 2

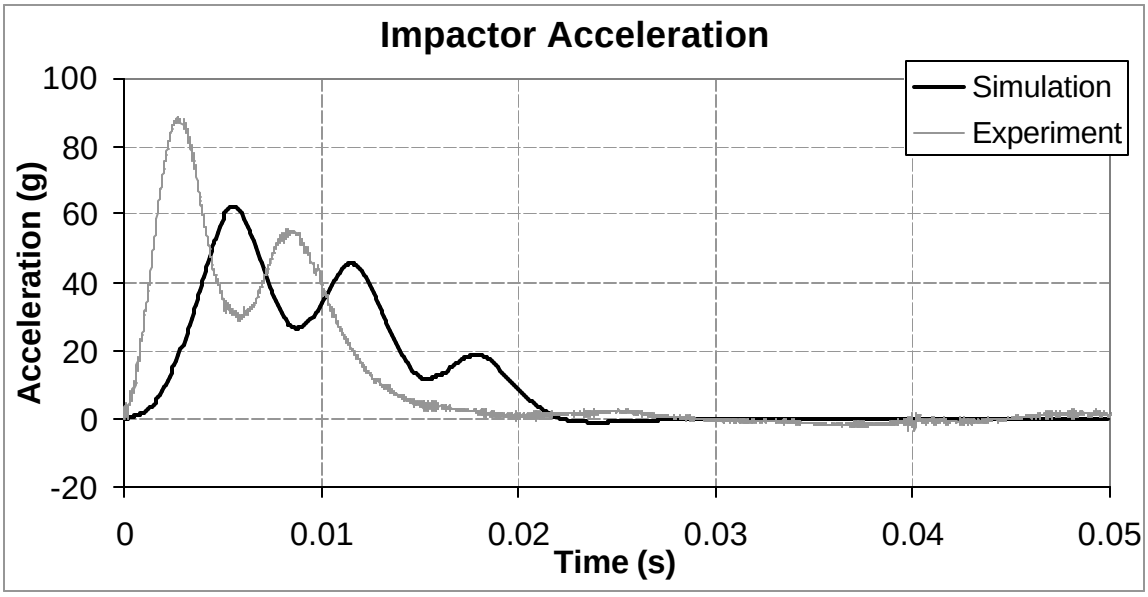

Figure 42. Heel Test 2: Impactor deceleration.

*The source of this rebound artifact has been identified, and is currently being addressed in the physical THOR-Lx design. The model is correct in not reproducing this artifact.

Note: All of the data from the simulations were resampled at 1000 Hz and then filtered with a CFC 60 (100 Hz) Butterworth 4 pole filter.

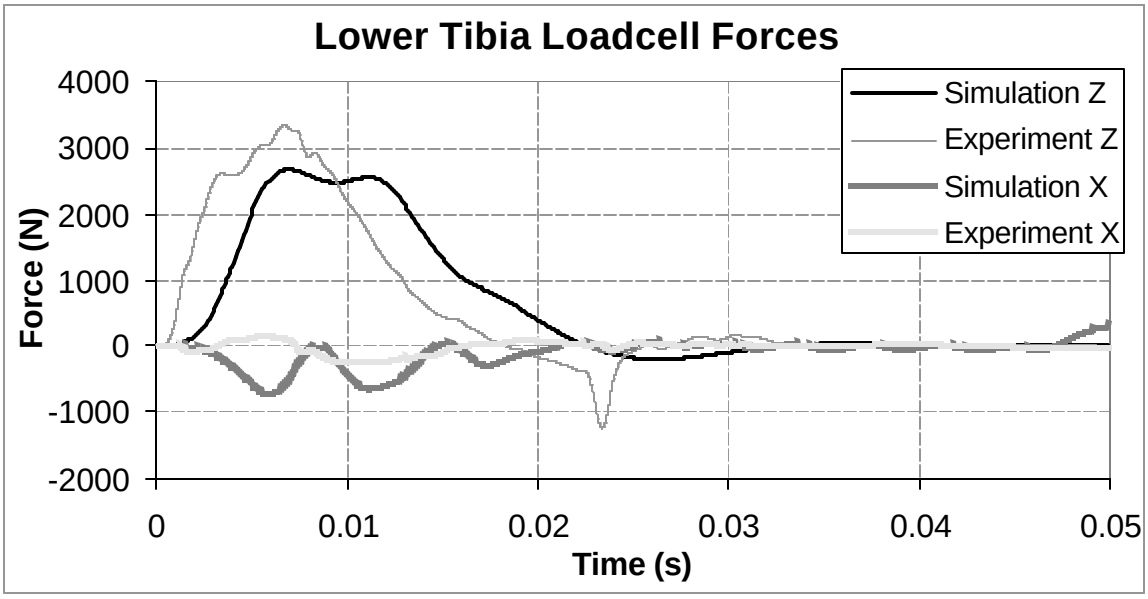

Figure 43. Heel Test 2: Lower tibia load cell forces.*

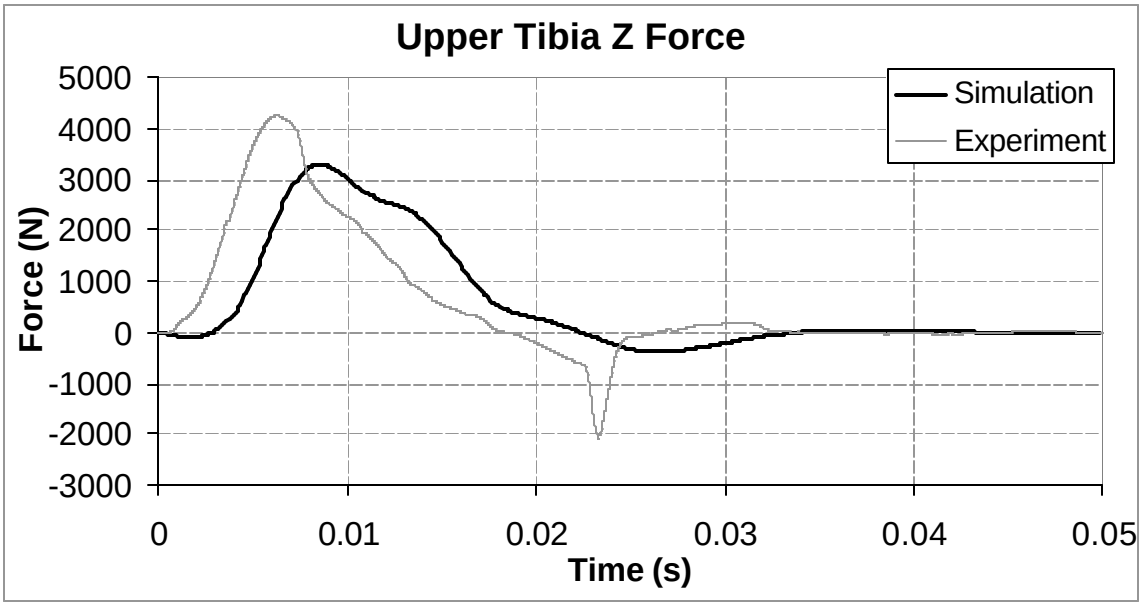

Figure 44. Heel Test 2: Upper tibia load cell forces.*

*The source of this rebound artifact has been identified, and is currently being addressed in the physical THOR-Lx design. The model is correct in not reproducing this artifact.

Note: All of the data from the simulations were resampled at 1000 Hz and then filtered with a CFC 60 (100 Hz) Butterworth 4 pole filter.

Achilles' Test 1

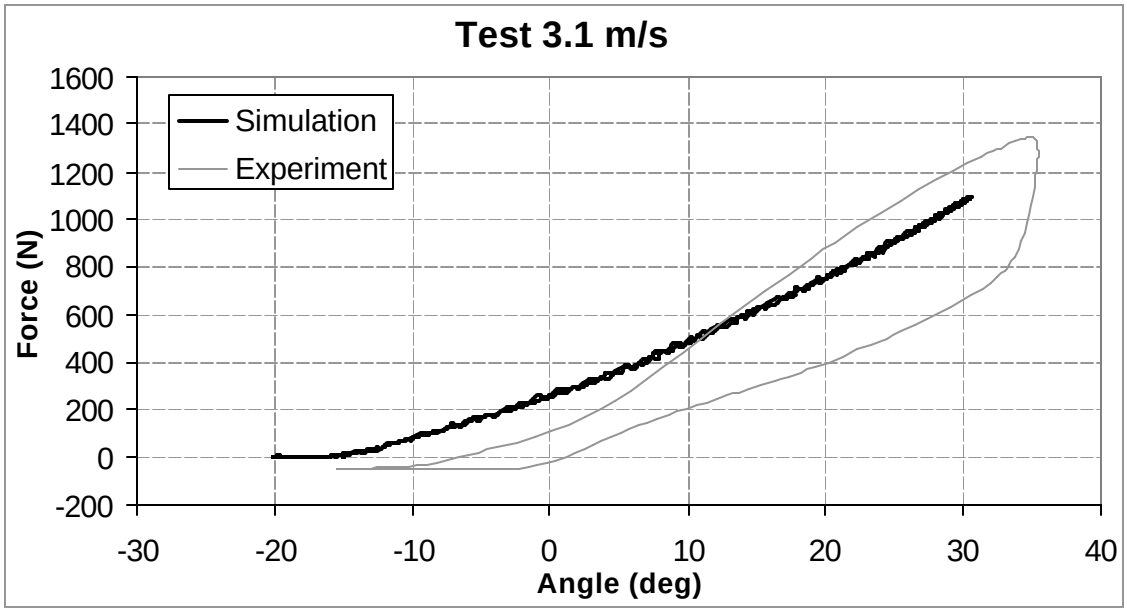

Figure 45. Achilles' Test 1: Achilles' Force.

Achilles' Test 2

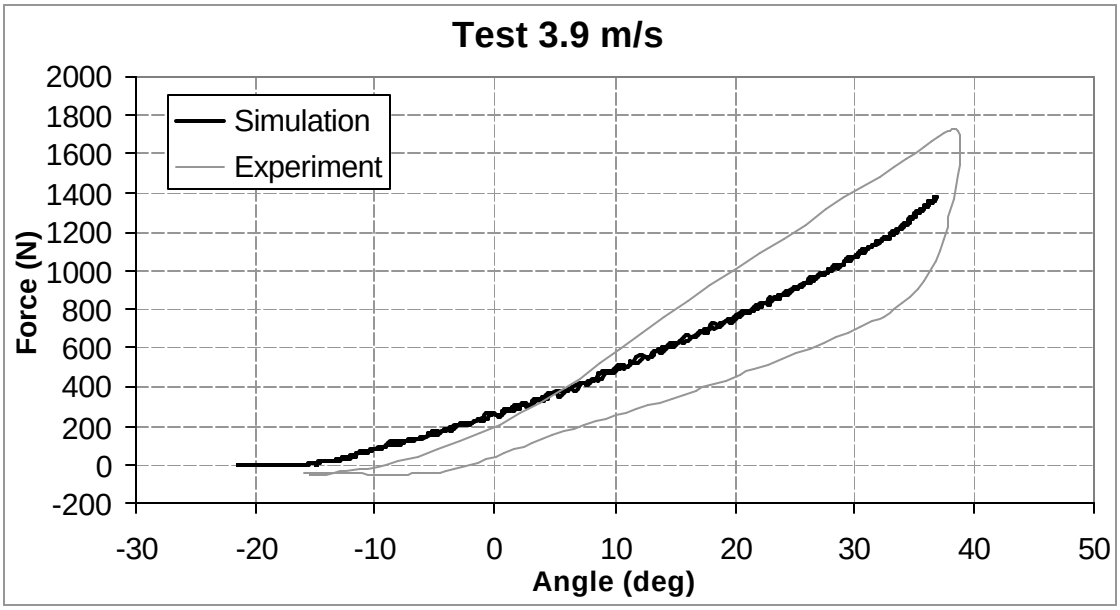

Figure 46. Achilles' Test 2: Achilles' Force.

Note: All of the data from the simulations were resampled at 1000 Hz and then filtered with a CFC 60 (100 Hz) Butterworth 4 pole filter.

Achilles' Test 3

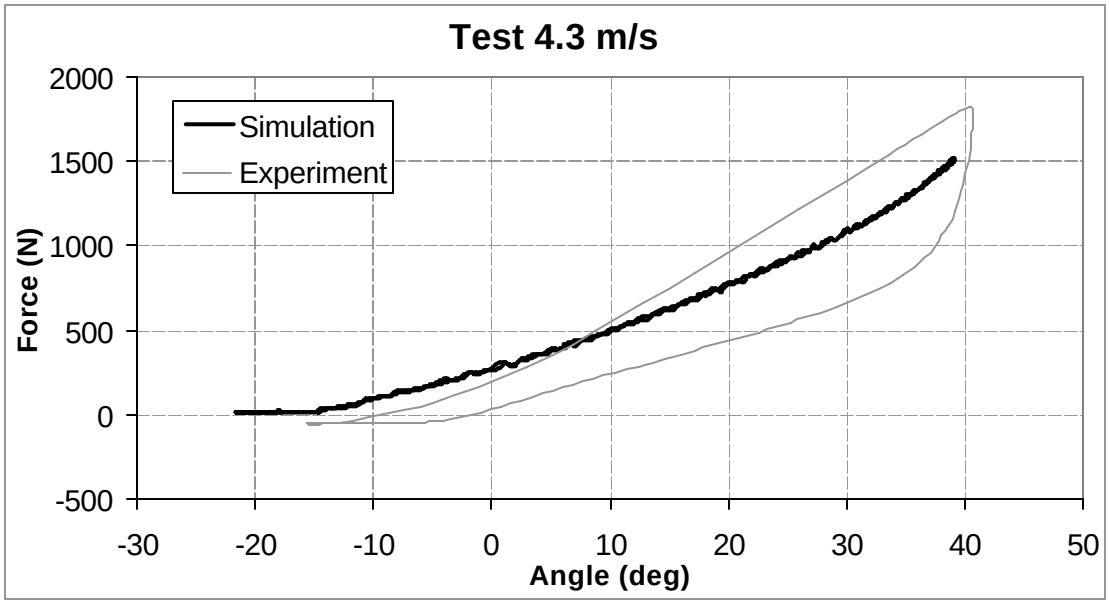

Figure 47. Achilles' Test 3: Achilles' Force.

Skin Test 1

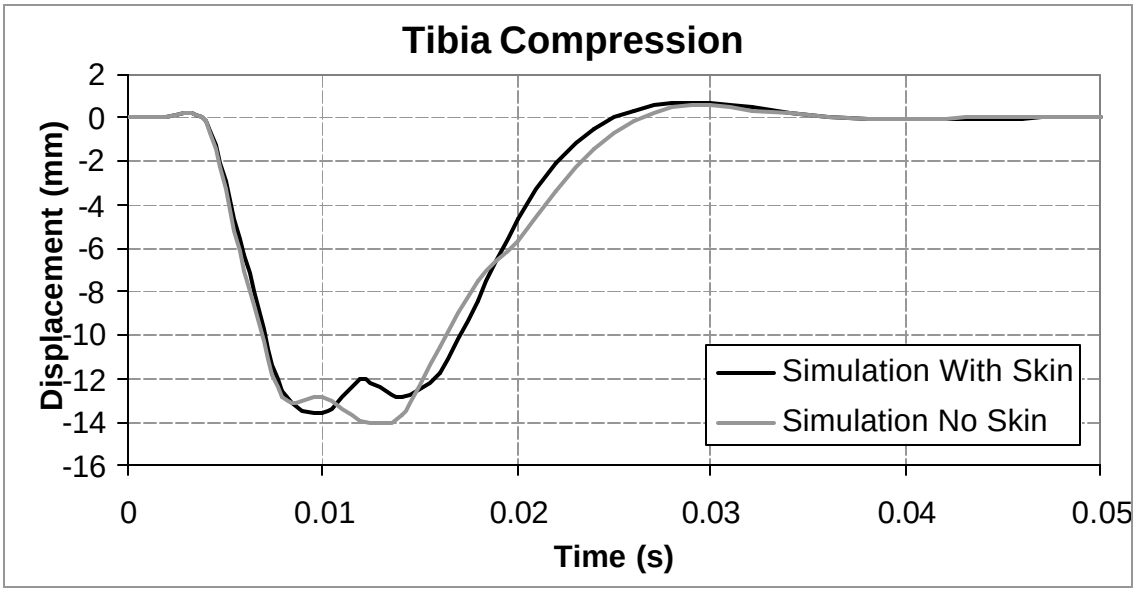

Figure 48. Skin Test 1: Tibia Compression.

Note: All of the data from the simulations were resampled at 1000 Hz and then filtered with a CFC 60 (100 Hz) Butterworth 4 pole filter.

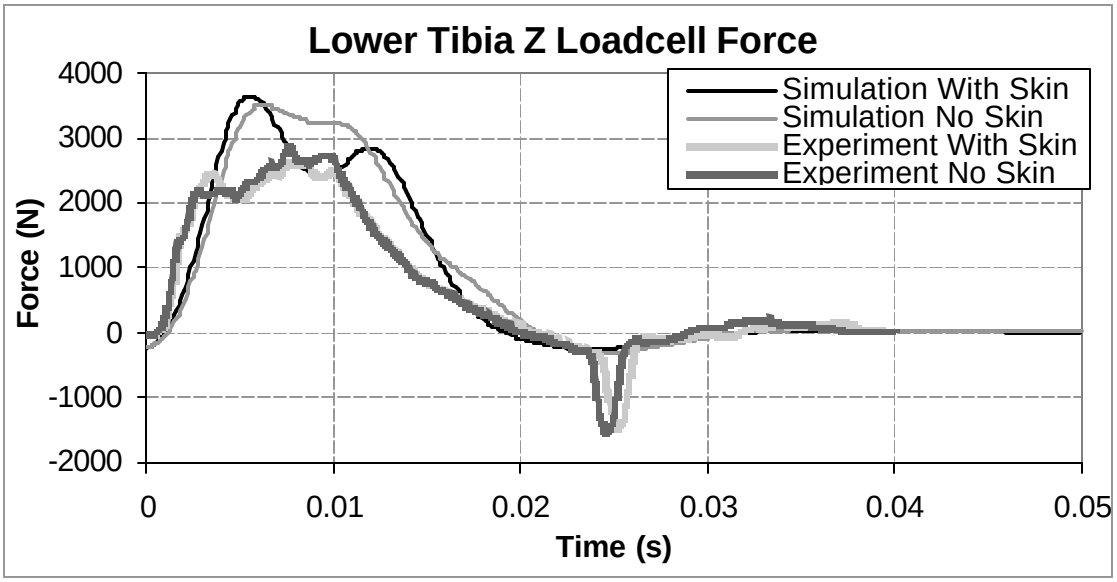

Figure 49. Skin Test 1: Lower tibia Z load cell forces.*

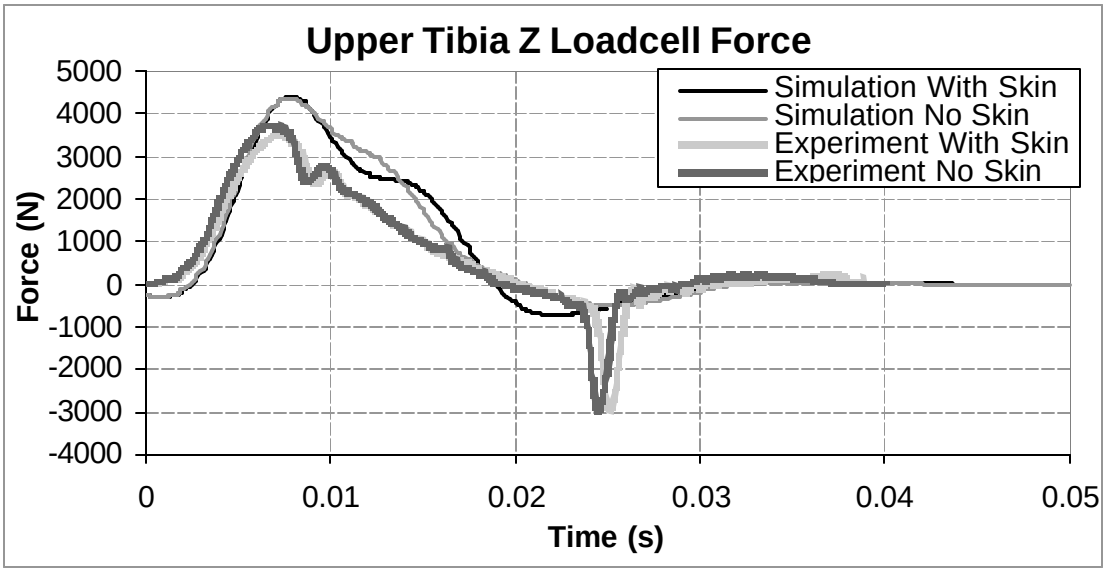

Figure 50. Skin Test 1: Upper tibia Z load cell forces.*

*The source of this rebound artifact has been identified, and is currently being addressed in the physical THOR-Lx design. The model is correct in not reproducing this artifact.

Note: All of the data from the simulations were resampled at 1000 Hz and then filtered with a CFC 60 (100 Hz) Butterworth 4 pole filter.

Skin Test 2

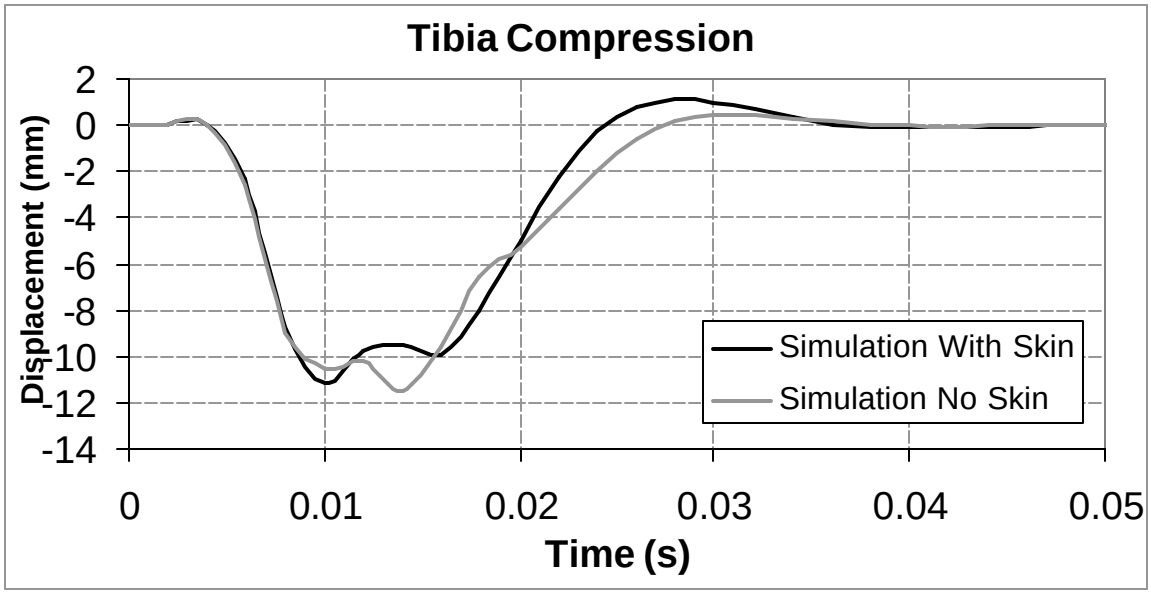

Figure 51. Skin Test 2: Tibia Compression.

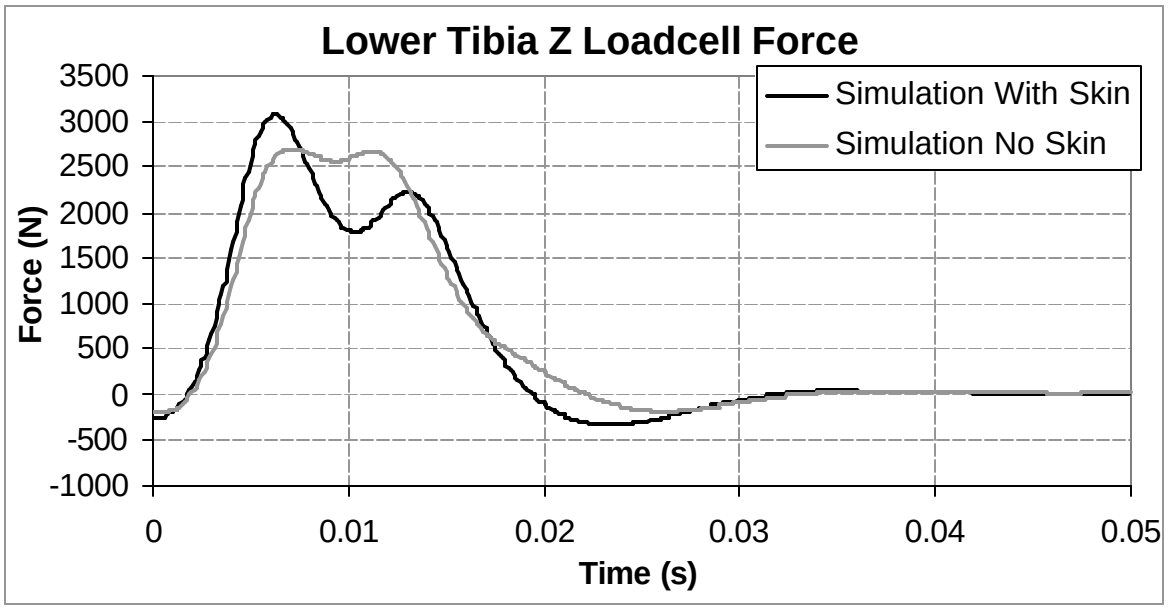

Figure 52. Skin Test 2: Lower tibia Z load cell forces.

Note: All of the data from the simulations were resampled at 1000 Hz and then filtered with a CFC 60 (100 Hz) Butterworth 4 pole filter.

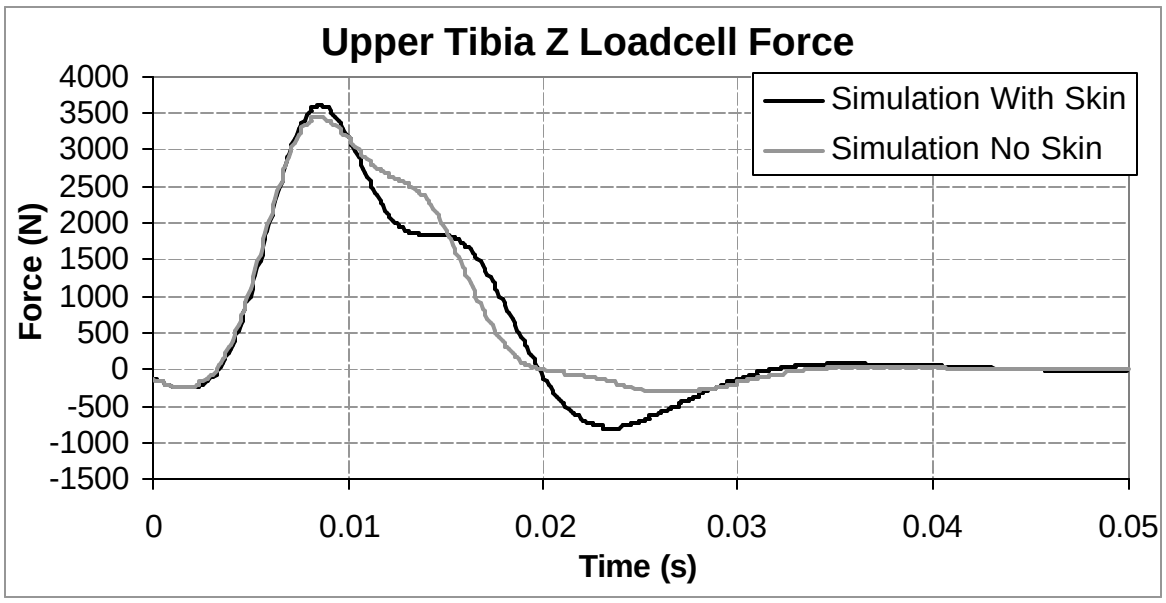

Figure 53. Skin Test 2: Upper tibia Z load cell forces.

Note: All of the data from the simulations were resampled at 1000 Hz and then filtered with a CFC 60 (100 Hz) Butterworth 4 pole filter.

APPENDIX II: FOOT POSITIONING

This appendix describes the procedure for rotating the foot in dorsiflexion or plantarflexion. Each rotation involves two main steps: 1) rotating the main parts and 2) adjusting the Achilles' cable.

First, select the elements of the parts and groups listed below (Note: DO NOT select the two internal-external rotation joints).

Parts	Parts
Torque_Base_CenterBlock_LH	Torque_Base_CenterBlock_RH
Eversion_Inversion_SoftStop_LH	Eversion_Inversion_SoftStop_RH
Evers_Invers_SoftStop_Base_LH	Evers_Invers_SoftStop_Base_RH
btm_Torque_Base_Cap_LH	btm_Torque_Base_Cap_RH
btm_Torque_Base_LH	btm_Torque_Base_RH
fraft_Ankle_Bushing_Plates_LH	fraft_Ankle_Bushing_Plates_RH
frnt_Ankle_PotentiomtrCover_LH	frnt_Ankle_PotentiomtrCover_RH
Foot_Composite_Sole_LH	Foot_Composite_Sole_RH
Heel_Padding_LH	Heel_Padding_RH
Foot_TriAxial_Mountng_Plate_LH	Foot_TriAxial_Mountng_Plate_RH
Foot_TriAccelerometer_LH	Foot_TriAccelerometer_RH
Foot_LH	Foot_RH
Achilles_Heel_Mountng_Post_LH	Achilles_Heel_Mountng_Post_RH
Achilles_lwr_Mountng_Post_LH	Achilles_lwr_Mountng_Post_RH
JNTS_revolute_ankle_LH	JNTS_revolute_ankle_RH

Groups	Groups
XN2RB_Achilles_lwr_mntngPost_LH	XN2RB_Achilles_lwr_mntngPost_RH
XN2RB_JNT_dorsiA_sdBplates_LH	XN2RB_JNT_dorsiA_sdBplates_RH
XN2RB_JNT_dorsiB_TqBsCntrblk_LH	XN2RB_JNT_dorsiB_TqBsCntrblk_RH
XN2RB_JNT_evrsA_faBshngPlts_LH	XN2RB_JNT_evrsA_faBshngPlts_LH
XN2RB_JNT_evrsB_TqBsCntrblk_LH	XN2RB_JNT_evrsB_TqBsCntrblk_RH

After selecting the parts and groups above, rotate the selected items about the global-Y axis using any end point of the dorsi-plantar flexion joint as the center of rotation. For example, rotation of +15 degrees would allow rotation from the neutral position of -15 degrees below horizontal to horizontal.

Next, find the angle formed by the following three points: Achilles' heel attachment point (node 507554), slip-ring (node 507503), and the loose end of the Achilles' cable (node 507555). The slip-ring is the vertex of the angle. Following the example above, the seatbelt elements should be rotated by +6.62 deg. Then, select the seatbelt (SB) elements between the slip-ring and bottom SB elements that are attached to the Achilles' lower mounting posts. Rotate the selected items about the global-Y axis using either of the two slip-rings as the center of rotation.

Finally, add SB elements so that all elements have the same length of 1.949 mm (only the bottom SB elements that are attached to the Achilles' lower mounting posts will have a length larger then 1.949 to make the elements fit evenly). Finish by equivalencing duplicate nodes and re-numbering consistently the new nodes and elements.

Note: For correlation heel impact, add the Torque Base Center Blocks into their respective legs' rigid body (RB) sets for the Top Torque Base.

APPENDIX III: MASS COMPARISON

Table 3. Comparison of masses in the THOR-LX FE model to the physical THOR-LX.

Location	Component Name	Physical Mass (kg)	FE Model Mass (kg)
Tibia:			
	Upper tibia load cell	0.475	0.550
	Lower tibia load cell	0.570	0.591
	Compliant assembly	0.290	0.274
	Knee clevis	0.250	0.237
	Upper tibia tube	0.070	0.058
	Lower tibia tube	0.220	0.180
	Achilles assembly	0.445	0.422
	Tibia skin	0.550	0.550
	Total mass of tibia (from knee clevis to ankle joint)	2.92	2.86
Foot:			
	Composite foot plate	0.110	0.177
	Achilles mounting plate	0.070	0.055
	Heel pad	0.040	0.035
	Foot skin	0.460	0.325
	Total mass of foot: (from ankle joint down)	0.540	0.504